

# Probing Type-I 2HDM light Higgs in the top-pair-associated diphoton channel

---

Yabo Dong,<sup>a</sup> Kun Wang,<sup>b,\*</sup> and Jingya Zhu<sup>a,\*</sup>

<sup>a</sup>*School of Physics and Electronics, Henan University, Kaifeng 475004, China*

<sup>b</sup>*College of Science, University of Shanghai for Science and Technology, Shanghai 200093, China*

*E-mail:* [dongyb@henu.edu.cn](mailto:dongyb@henu.edu.cn), [kwang@usst.edu.cn](mailto:kwang@usst.edu.cn), [zhuji@henu.edu.cn](mailto:zhuji@henu.edu.cn)

**ABSTRACT:** In this study, we investigate the potential of the Type-I Two-Higgs-Doublet Model (2HDM-I) to account for the 95 GeV diphoton excess observed at the LHC, under current theoretical and experimental constraints. Monte Carlo (MC) simulations are performed for the process  $pp \rightarrow t(\rightarrow W^+b)\bar{t}(\rightarrow W^-\bar{b})h(\rightarrow \gamma\gamma)$  to evaluate the discovery potential of a 95 GeV Higgs boson at future colliders. The analysis shows that direct Higgs search data impose strong constraints on the model parameter  $\alpha$ , excluding parameter space with  $\alpha \lesssim 0.95$ . The diphoton excess observed by CMS and ATLAS can be explained by samples with  $\sin(\beta - \alpha) \approx -0.2$  or  $\sin(\beta - \alpha) \approx 0.35$ . According to the MC results, a statistical significance of  $2\sigma$  can be reached at the HL-LHC with an integrated luminosity of  $L = 764 \text{ fb}^{-1}$ , while achieving  $5\sigma$  significance at the HL-LHC is not feasible. At the HE-LHC,  $2\sigma$  and  $5\sigma$  significance levels require integrated luminosities of at least  $L = 390 \text{ fb}^{-1}$  and  $L = 2.4 \text{ ab}^{-1}$ , respectively. The same levels of significance can be achieved at the FCC-hh with significantly lower luminosities:  $L = 36 \text{ fb}^{-1}$  for  $2\sigma$  and  $L = 227 \text{ fb}^{-1}$  for  $5\sigma$ . Parameter points with  $\sin(\beta - \alpha) \approx 0$  remain difficult to probe in diphoton channel, even with further increases in collider energy and luminosity.

ARXIV EPRINT: [2410.13636](https://arxiv.org/abs/2410.13636)

---

\*Corresponding author.

---

## Contents

<b>1</b>	<b>Introduction</b>	<b>1</b>
<b>2</b>	<b>The two-Higgs doublet model</b>	<b>3</b>
<b>3</b>	<b>Parameters scan and constraints</b>	<b>4</b>
<b>4</b>	<b>The discussion of parameter space scan results</b>	<b>6</b>
<b>5</b>	<b>Future collider simulations and discussion</b>	<b>12</b>
<b>6</b>	<b>Conclusions</b>	<b>19</b>

---

## 1 Introduction

The primary goal of the LHC is to search for the Higgs boson and hypothetical particles beyond the Standard Model (BSM). After the decisive discovery of the 125 GeV Higgs boson by the CMS [1] and ATLAS [2] collaborations in 2012, subsequent measurements have confirmed its mass, spin, width, and couplings [3, 4], largely confirming the predictions of the Standard Model (SM). While the SM remains robust under these experimental validations, the absence of new particle discoveries significantly restricts the parameter space of BSM theories. Nevertheless, persistent anomalies and excess signals observed in experiments at LEP, Tevatron, and LHC hint at the presence of new physics, underscoring the importance of continued investigations into BSM theories. These studies are crucial for defining the limits of the SM and guiding future theoretical and experimental efforts.

As early as 2003, the LEP experiment documented a  $2.3\sigma$  local excess in the  $e^+e^- \rightarrow Z(h \rightarrow b\bar{b})$  channel at about 98 GeV [5]. In 2018, the CMS collaboration combined data from 8 TeV ( $19.7 \text{ fb}^{-1}$ ) and 13 TeV ( $35.9 \text{ fb}^{-1}$ ) runs to report a  $h \rightarrow \gamma\gamma$  excess for a mass of 95.3 GeV with the local (global) significance of  $2.8\sigma$  ( $1.3\sigma$ ), respectively [6]. More recently, in 2023, ATLAS reported a  $1.7\sigma$  excess at a mass of 95.4 GeV in the  $h \rightarrow \gamma\gamma$  channel [7]. In 2024, CMS reported a local (global) significance of  $2.9\sigma$  ( $1.3\sigma$ ) for the same mass hypothesis [8]. At the closely related diphoton invariant mass points of 95.4 GeV and 95.3 GeV, both ATLAS and CMS have reported a persistent signal excess. This excess has shown no sign of diminishing over time, strongly suggesting the possible existence of a scalar particle around 95 GeV in the diphoton channel.

The reported 95 GeV excess has attracted considerable theoretical interest as a possible signal of new physics [9–17]. Recent investigations have meticulously examined this phenomenon across various models, focusing on the presence of a light scalar. These models include the simple SM extensions [18–20], the minimal dilaton model [21, 22], the two Higgs doublet model (2HDM) with a singlet extensions [23–27], the next-to-minimal two

Higgs doublet model and its extensions [28–31], the Georgi-Machacek model [32–34], the next-to-minimal supersymmetric model [35–45] and its semi-constrained version [46], etc. For the model of these studies, the light scalar is usually singlet-dominated, mixing in part with the doublet Higgs. On the contrary, less attention has been paid to the model with a doublet-dominated scalar.

In this study, we explore the 2HDM, an additional  $SU(2)_L$  Higgs doublet extension of the SM that includes a second Higgs doublet [47–52], to give a correlation explanation of the doublet-dominated scalar. The primary rationale for introducing a second Higgs doublet is rooted in the insufficiency of a single doublet to both endow up-type and down-type quarks with mass and to eliminate anomalies inherent in supersymmetry [53]. The theoretical framework of 2HDM predicts a pseudoscalar Higgs boson, a pair of charged Higgs bosons, and two neutral scalar Higgs bosons. The pseudoscalar Higgs or one of the two neutral scalar Higgs can be a candidate to explain the 95 GeV excess in the experiments. Meanwhile, the inclusion of charged Higgs bosons and pseudoscalar in the 2HDM enriches the phenomenological landscape, offering diverse decay modes and branching ratios beyond those in the SM.

However, the 2HDM is particularly affected by experimental constraints due to its potential role in mediating flavor-changing neutral currents (FCNCs). To mitigate these effects, several variants of the 2HDM have been proposed [54, 55], including type-I (2HDM-I), type-II (2HDM-II), lepton-specific (2HDM-LS), and a flipped model (2HDM-Flipped), etc. Specifically, in the 2HDM-I [51, 56–59], a unique characteristic is that only one scalar doublet  $\Phi_2$  couple to quarks and leptons. According to its coupling characteristics, 2HDM-I has some interesting features. For example, only 2HDM-I can predict light neutral scalar  $h$  and charged scalar  $H^\pm$  under current theoretical and experimental constraints. Meanwhile, the light  $H^\pm$  can give an additional contribution to the process of  $h \rightarrow \gamma\gamma$  through the loop effect, thereby increasing the decay of  $h$  to diphoton and impress other decays [60]. Consequently, the light neutral scalar  $h$  in 2HDM-I may be an outstanding candidate to explain the 95 GeV diphoton excess and this work primarily explores such phenomenology of 2HDM-I.

Top-pair-associated channel can effectively reduce the SM QCD backgrounds by providing more final state tags. It is meaningful to study this channel, especially after the SM-like Higgs is confirmed in this channel [61, 62]. Therefore, this work focuses on the top-pair-associated diphoton channel. In this research, we explore the parameter space of the 2HDM-I model, evaluating its viability under current constraints to accommodate a 95 GeV light Higgs boson. Following this analysis, we perform Monte Carlo (MC) simulations to predict the feasibility of testing this model in future collider experiments, with a focus on the top-pair-associated diphoton channel.

The organization of this paper is as follows. In Sec. 2, we provide a brief overview of the 2HDM-I model and the relevant theoretical and experimental constraints. Sec. 3 shows the region of the parameter space scan and the constraints taken into account. In Sec. 4, we analyze the relevant phenomenology of the parameter space, compare the results with experimental data, and discuss their implications. In Sec. 5, we conduct collider simulations and analyze the results. In Sec. 6, we present our conclusions.

## 2 The two-Higgs doublet model

The 2HDM is a widely accepted and straightforward extension of the SM. The most general scalar potential in this model includes 14 additional parameters. Assuming CP conservation in the Higgs sector, it involves two complex doublets,  $\Phi_1$  and  $\Phi_2$ , each with a hypercharge  $Y = +1$ . The scalar potential is given by [47–49]:

$$V(\Phi_1, \Phi_2) = m_{11}^2 \Phi_1^\dagger \Phi_1 + m_{22}^2 \Phi_2^\dagger \Phi_2 - m_{12}^2 \left( \Phi_1^\dagger \Phi_2 + \text{h.c.} \right) + \frac{\lambda_1}{2} \left( \Phi_1^\dagger \Phi_1 \right)^2 + \frac{\lambda_2}{2} \left( \Phi_2^\dagger \Phi_2 \right)^2 + \lambda_3 \Phi_1^\dagger \Phi_1 \Phi_2^\dagger \Phi_2 + \lambda_4 \Phi_1^\dagger \Phi_2 \Phi_2^\dagger \Phi_1 + \frac{\lambda_5}{2} \left[ \left( \Phi_1^\dagger \Phi_2 \right)^2 + \text{h.c.} \right], \quad (2.1)$$

where  $m_{11}^2$ ,  $m_{12}^2$ ,  $m_{22}^2$ , and  $\lambda_i (i = 1, 2, \dots, 5)$  are real parameters. The model contains two complex scalar SU(2) doublets, which are defined as

$$\Phi_i = \begin{pmatrix} \phi_i^+ \\ (v_i + \phi_i + i\eta_i) / \sqrt{2} \end{pmatrix}, \quad i = 1, 2. \quad (2.2)$$

where  $v_i$  is the vacuum expectation values (VEVs) of  $\Phi_i$ , with  $\sqrt{v_1^2 + v_2^2} \equiv v \approx 246$  GeV.

The free parameters can then be traded for a more physically meaningful set:  $m_h$ ,  $m_H$ ,  $m_A$ ,  $m_{H^\pm}$ ,  $m_{12}^2$ ,  $\alpha$ , and  $\tan \beta$ . Here,  $m_h$  and  $m_H$  denote the masses of two neutral scalar Higgs bosons,  $m_A$  represents the pseudoscalar Higgs mass, and  $m_{H^\pm}$  is the mass of the charged Higgs boson. In addition,  $\alpha$  denotes the mixing angle of two neutral Higgs, while  $\tan \beta$  is defined as the ratio of the VEVs of  $\Phi_2$  and  $\Phi_1$ , expressed as  $\tan \beta \equiv v_2/v_1$ . The lighter  $h$  and heavier  $H$  are orthogonal combinations of  $\phi_1$  and  $\phi_2$  and can be given by:

$$h = \phi_1 \sin \alpha - \phi_2 \cos \alpha, \quad H = \phi_1 \cos \alpha + \phi_2 \sin \alpha. \quad (2.3)$$

The masses  $m_{H^\pm}$  and  $m_A$  are specified as follows [48]:

$$m_{H^\pm} = \sqrt{\frac{m_{12}^2 - (\lambda_4 + \lambda_5)v_1v_2}{v_1v_2}(v_1^2 + v_2^2)}, \quad m_A = \sqrt{\frac{m_{12}^2 - 2\lambda_5v_1v_2}{v_1v_2}(v_1^2 + v_2^2)}. \quad (2.4)$$

It follows that, under the assumption  $m_{H^\pm} = m_A$ , the parameters  $\lambda_4$  and  $\lambda_5$  are equal.

In the 2HDM-I, the Yukawa couplings of the up-type quarks  $u_R^i$ , the down-type quarks  $d_R^i$ , and the leptons  $e_R^i$  are all assumed to couple exclusively to  $\Phi_2$ , effectively eliminating all tree-level flavor-changing neutral currents (FCNCs) [54, 55]. Consequently, the Yukawa terms for the 2HDM-I Lagrangian based on the mass-eigenstate can be expressed as [63]

$$\mathcal{L}_{\text{Yukawa}} = - \sum_{f=u,d,\ell} \frac{m_f}{v} \left( \xi_h^f \bar{f} f h + \xi_H^f \bar{f} f H - i \xi_A^f \bar{f} \gamma_5 f A \right) - \left\{ \frac{\sqrt{2} V_{ud}}{v} \bar{u} \left( m_u \xi_A^u P_L + m_d \xi_A^d P_R \right) d H^+ + \frac{\sqrt{2} m_\ell \xi_A^\ell}{v} \bar{\nu}_L \ell_R H^+ + \text{h.c.} \right\}, \quad (2.5)$$

where  $P_{R,L} = (1 \pm \gamma_5)/2$ ,  $\xi_h^{u,d,\ell} = \cos \alpha / \sin \beta$ ,  $\xi_H^{u,d,\ell} = \sin \alpha / \sin \beta$ ,  $\xi_A^u = \cot \beta$  and  $\xi_h^{d,\ell} = -\cot \beta$ . The couplings of Higgs to fermions and bosons in THDM-I are similar to those in

SM, except for extra coefficients [64]. Combined with Eq. (2.5), the couplings of the light and heavy neutral Higgs bosons ( $h$  and  $H$ ) to the vector bosons  $VV$  ( $VV = WW, ZZ$ ) in THDM-I,  $C_{hVV}$  and  $C_{HVV}$ , can be derived as follows:

$$C_{hVV} = C_{hVV}^{\text{SM}} \times \sin(\beta - \alpha), \quad C_{HVV} = C_{HVV}^{\text{SM}} \times \cos(\beta - \alpha). \quad (2.6)$$

The couplings of  $h$  and  $H$  to fermions in THDM-I,  $C_{hff}$  and  $C_{Hff}$ , can be derived as follows:

$$C_{hff} = C_{hff}^{\text{SM}} \times \cos \alpha / \sin \beta, \quad C_{Hff} = C_{Hff}^{\text{SM}} \times \sin \alpha / \sin \beta. \quad (2.7)$$

The decay width of the light Higgs to  $\gamma\gamma$ , denoted as  $\Gamma(h \rightarrow \gamma\gamma)$ , is given as [60, 65]

$$\Gamma(h \rightarrow \gamma\gamma) = \frac{G_F \alpha^2 m_h^3}{128 \sqrt{2} \pi^3} \left| \sum_{f \in \{t, b\}} C_f Q_f^2 N_c A_{1/2}(\tau_f) + C_W A_1(\tau_W) + C_{H^\pm} A_0(\tau_{H^\pm}) \right|^2. \quad (2.8)$$

Here,  $C_W = C_{hWW}/C_{hWW}^{\text{SM}}$  represents the ratio of Higgs to  $W$  boson coupling in the 2HDM relative to that of the SM, and  $C_f = C_{hff}/C_{hff}^{\text{SM}}$  signifies the corresponding ratio for fermion couplings. Furthermore,  $C_{H^\pm} = -m_W/gm_{H^\pm}^2 \times C_{hH^+H^-}$ , where  $C_{hH^+H^-}$  is the coupling between  $h$  and  $H^\pm$ , the detailed information can be obtained from Ref. [66]. With  $\tau_i = m_h^2/(4m_i^2)$  (for  $i = f, W, H^\pm$ ) denotes the normalized mass terms, the functions  $A_0, A_{1/2}, A_1$  are defined as follows:

$$\begin{aligned} A_0(\tau_{H^\pm}) &= -[\tau_{H^\pm} - f(\tau_{H^\pm})]\tau_{H^\pm}^{-2}, \\ A_{1/2}(\tau_f) &= 2[\tau_f + (\tau_f - 1)f(\tau_f)]\tau_f^{-2}, \\ A_1(\tau_W) &= -[2\tau_W^2 + 3\tau_W + 3(2\tau_W - 1)f(\tau_W)]\tau_W^{-2}, \end{aligned} \quad (2.9)$$

where

$$f(\tau) = \begin{cases} \arcsin^2 \sqrt{\tau} & , \quad \tau \leq 1 \\ -\frac{1}{4} \left[ \log \frac{1+\sqrt{1-\tau^{-1}}}{1-\sqrt{1-\tau^{-1}}} - i\pi \right]^2 & , \quad \tau > 1 \end{cases}. \quad (2.10)$$

### 3 Parameters scan and constraints

We use the Mathematica package SARAH-4.15.2 [67–70] to generate the model file and then use the package SPheno-4.0.5 [71, 72] to calculate the particle spectrum. The seven input parameters are  $m_h, m_H, m_A, m_{H^\pm}, m_{12}^2, \alpha$ , and  $\tan \beta$ . Since one of the CP-even Higgs bosons should be the SM-like, we denote  $H$  as the SM-like Higgs with  $m_H = 125$  GeV. The mass of  $h$  is set to 95 GeV. The other parameters are explored within the following ranges:

$$\begin{aligned} \alpha &\in [-\pi/2, \pi/2], \\ \tan \beta &\in [0, 20], \\ m_{12} &\in [-10 \text{ TeV}, 10 \text{ TeV}], \\ m_{H^\pm} = m_A &\in [150 \text{ GeV}, 1000 \text{ GeV}]. \end{aligned} \quad (3.1)$$

For the experimental constraints, we consider the following:

- Constraints from B physics,  $B_d \rightarrow \mu^+ \mu^-$ ,  $B_s \rightarrow \mu^+ \mu^-$  and  $B \rightarrow X_s \gamma$  [73–77]:

$$\begin{aligned} \text{BR}(B_d \rightarrow \mu^+ \mu^-) &< 2.1 \times 10^{-10}, \\ \text{BR}(B_s \rightarrow \mu^+ \mu^-) &= (2.9 \pm 0.8) \times 10^{-9}, \\ \text{BR}(B \rightarrow X_s \gamma) &= (3.32 \pm 0.3) \times 10^{-4}. \end{aligned} \quad (3.2)$$

The package `SuperIso-v4.1` [78, 79] is used to calculate the branching ratios related to B physics.

- The muon magnetic moment predicted by the SM,  $a_\mu^{\text{SM}}$ , is given by [80]:

$$a_\mu^{\text{SM}} = 116591810(43) \times 10^{-11}. \quad (3.3)$$

The latest experimental result from the Fermi National Accelerator Laboratory (FNAL) [81], denoted as  $a_\mu^{\text{exp}}$ , is :

$$a_\mu^{\text{exp}} = 116592059(22) \times 10^{-11}. \quad (3.4)$$

There is a deviation of approximately  $5\sigma$  between the experimental measurement and the SM prediction. The difference is given by [82]:

$$\Delta a_\mu \equiv a_\mu^{\text{exp}} - a_\mu^{\text{SM}} = (24.9 \pm 4.8) \times 10^{-10}. \quad (3.5)$$

The value of  $\Delta a_\mu$  is calculated at the two-loop level using the `GM2Calc-2.2.0` package [83, 84].

- Constraints from direct Higgs searches in the diphoton channel, such as  $e^+e^- \rightarrow ZH (\rightarrow \gamma\gamma)$  at LEP [85] and  $pp \rightarrow h \rightarrow \gamma\gamma$  at the LHC [6, 8, 86, 87], are taken into account. Additional constraints from other search channels are evaluated at the 95% confidence level using the `HiggsBounds-5.10.0` package [88].
- Constraints from SM-like Higgs data are applied by testing the 125 GeV Higgs boson in the 2HDM-I using the `HiggsSignal-2.6.0` package [89]. This package computes a  $\chi^2$  value using the peak-centered  $\chi^2$  method to evaluate the compatibility of the SM-like 125 GeV Higgs with experimental measurements. For 107 degrees of freedom, a  $\chi^2$  value less than 124.3 is required at the 95% confidence level.
- Constraints from electroweak precision observables [90, 91] requiring that the oblique parameters  $S$ ,  $T$ , and  $U$  to matching the global fit results as detailed in [77]:

$$S = -0.04 \pm 0.10, \quad T = 0.01 \pm 0.12, \quad U = -0.01 \pm 0.09, \quad (3.6)$$

where the correlation coefficients are given as  $\rho_{ST} = 0.92$ ,  $\rho_{SU} = -0.80$ , and  $\rho_{TU} = -0.93$ .

For theoretical constraints, we account for the following:

- Constraints from unitarity on scalar parameters requiring that the scalar couplings  $\lambda_i$  (where  $i = 1, 2, \dots, 5$ ) to satisfy specific conditions [92–94]:

$$\begin{aligned}
& \left| 2\lambda_3 + \frac{\lambda_5}{2} \right| \leq 8\pi, \quad \left| 2\lambda_3 \pm \lambda_4 - \frac{\lambda_5}{2} \right| \leq 8\pi, \quad \left| 2\lambda_3 + \lambda_4 - \frac{\lambda_5}{2} \right| \leq 8\pi, \\
& \left| 2\lambda_3 - \lambda_4 - \frac{5\lambda_5}{2} \right| \leq 8\pi, \quad \left| 2\lambda_3 + 2\lambda_4 - \frac{\lambda_5}{2} \right| \leq 8\pi, \\
& \left| \lambda_1 + \lambda_2 + 2\lambda_3 \pm \sqrt{(\lambda_1 - \lambda_2)^2 + \frac{1}{4}\lambda_5^2} \right| \leq 8\pi, \\
& \left| \lambda_1 + \lambda_2 + 2\lambda_3 \pm \sqrt{(\lambda_1 - \lambda_2)^2 + \frac{1}{4}(-2\lambda_4 + \lambda_5)^2} \right| \leq 8\pi, \\
& \left| 3(\lambda_1 + \lambda_2 + 2\lambda_3) \pm \sqrt{9(\lambda_1 - \lambda_2)^2 + \left(4\lambda_3 + \lambda_4 + \frac{1}{2}\lambda_5\right)^2} \right| \leq 8\pi.
\end{aligned} \tag{3.7}$$

- Constraints from vacuum stability, as outlined in [95]:

$$\lambda_1, \lambda_2 > 0, \quad \lambda_3 > -\sqrt{\lambda_1\lambda_2}, \quad \lambda_3 + \min[0, \lambda_4 - |\lambda_5|] > -\sqrt{\lambda_1\lambda_2}. \tag{3.8}$$

- Constraints from perturbativity, as outlined in [48], requiring that the absolute values of the scalar couplings  $\lambda_i$  (for  $i = 1, 2, \dots, 5$ ) to be less than  $8\pi$ , specifically,  $|\lambda_i| < 8\pi$ .

#### 4 The discussion of parameter space scan results

In Fig. 1, the surviving samples are shown in the  $\tan\beta$  versus  $\alpha$  planes (upper panels) and in the  $|m_{12}|$  versus  $m_A$  planes (lower panels), with colors indicating the  $\chi^2$  in the left, the branching ratio of  $B \rightarrow X_s\gamma$  in the middle, and the muon anomalous magnetic moment  $\Delta a_\mu$  in the right. The light gray samples are excluded based on Higgs direct search data, primarily due to the strong coupling of  $h$  to fermions when  $\cos\alpha$  is large and  $\sin\alpha$  is small. The light blue samples are excluded for failing to provide an appropriate muon anomalous magnetic moment, and the gray samples are excluded based on  $\text{Br}(B \rightarrow X_s\gamma)$  data. The results of the parameter space scan indicate that direct searches for BSM Higgs bosons impose strong constraints on  $\alpha$ , excluding all samples with  $\alpha \lesssim 0.95$ . One can draw several conclusions from Fig. 1:

- From the left two panels of Fig. 1, one can observe that  $\alpha$  has a significant impact on the  $\chi^2$  value, while  $\tan\beta$ ,  $m_{12}$ , and  $m_A$  exhibit only a minor influence. The  $\chi^2$  is computed to assess the compatibility of the 125 GeV SM-like Higgs boson with experimental data. This compatibility is primarily determined by the Higgs couplings to gauge bosons and fermions, which are strongly dependent on the mixing angle  $\alpha$ . The minimum  $\chi^2$  value, approximately 85, is achieved around  $\alpha \approx 1.05$ , suggesting that the SM-like Higgs boson in this region is in good agreement with current Higgs measurements.

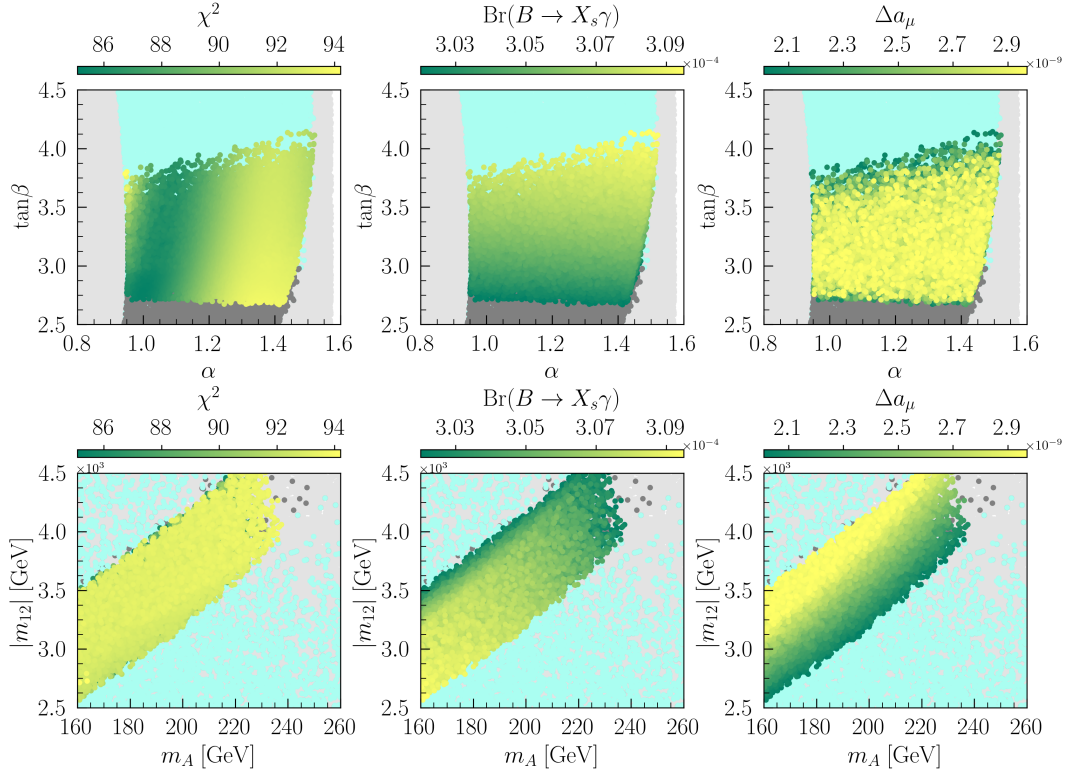


**Figure 1.** The surviving samples in the  $\tan\beta$  versus  $\alpha$  (upper panels) and  $|m_{12}|$  versus  $m_A$  planes (lower panels), with colors indicating the  $\chi^2$  (left), the branching ratio  $\text{Br}(B \rightarrow X_s\gamma)$  (middle), and the muon anomalous magnetic moment  $\Delta a_\mu$  (right). The light gray samples are excluded by direct Higgs searches, the light blue samples are excluded for failing to provide an appropriate muon anomalous magnetic moment, and the gray samples are excluded based on  $\text{Br}(B \rightarrow X_s\gamma)$  data.

- From the middle two panels of Fig. 1, one can observe that the branching ratio  $\text{Br}(B \rightarrow X_s\gamma)$  strongly depends on  $\tan\beta$ , and is nearly proportional to it. The surviving samples are required to satisfy  $\tan\beta \gtrsim 2.6$  in order to be consistent with experimental constraints; those that do not meet this condition are excluded. Moreover, smaller values of  $m_A$  and  $|m_{12}|$  tend to enhance  $\text{Br}(B \rightarrow X_s\gamma)$  at fixed  $\tan\beta$ .
- From the right two panels of Fig. 1, it is evident that a larger  $|m_{12}|$  tends to predict a larger  $\Delta a_\mu$ , whereas a heavier  $m_A$  leads to a smaller  $\Delta a_\mu$ . In general, samples satisfying  $|m_{12}| \gtrsim 18 m_A - 400$  GeV and  $|m_{12}| \lesssim 18 m_A + 600$  GeV can yield a  $\Delta a_\mu$  value consistent with experimental observations. Moreover, the muon anomalous magnetic moment also imposes an upper bound on  $\tan\beta$ ; samples with  $\tan\beta \gtrsim 4$  fail to produce a sufficiently large  $\Delta a_\mu$  and are thus excluded.
- By examining the right four panels of Fig. 1, one can observe that achieving a larger  $\text{Br}(B \rightarrow X_s\gamma)$  generally requires a larger  $\tan\beta$ , a smaller  $|m_{12}|$ , and a lighter  $m_A$ . However, satisfying the muon anomalous magnetic moment data impose conflicting constraints, requiring that  $\tan\beta$  not be too large and  $|m_{12}|$  not be too small. As a

result, if one aims to obtain a larger  $\text{Br}(B \rightarrow X_s \gamma)$ , the constraints from the muon anomalous magnetic moment should be appropriately relaxed. The samples have been explicitly checked to confirm that this behavior holds as expected.

- From the lower right panel of Fig. 1, it is evident that larger  $|m_{12}|$  contributes positively to  $\Delta a_\mu$ , whereas larger  $m_A$  contributes negatively. This effect arises from additional corrections to the pseudoscalar  $A$  induced by one-loop diagrams [96–99], which are expressed as

$$\Delta a_\mu^{1L} = \frac{m_\mu m_\tau \rho^2}{8\pi^2} \left[ \frac{(\log \frac{m_H^2}{m_\tau^2} - \frac{3}{2})}{m_H^2} - \frac{\log(\frac{m_A^2}{m_\tau^2} - \frac{3}{2})}{m_A^2} \right], \quad (4.1)$$

where  $\rho$  is the coupling parameter for  $\mu$  and  $\tau$  to  $H$  and  $A$ . It can be seen that  $\Delta a_\mu$  gets a positive contribution at the one-loop level only if  $m_A$  is greater than  $m_H$ . In our calculations,  $m_A$  is not significantly larger than  $m_H$ , so the term inside the square brackets is about  $10^{-4}$ , and the term before the square brackets is about  $10^{-8}$ . Consequently, the net contribution from one-loop processes is about  $10^{-12}$ . The two-loop contributions to  $\Delta a_\mu$  are divided into bosonic ( $a_\mu^B$ ) and fermionic ( $a_\mu^F$ ) parts, as detailed in [100–102], which given by

$$\Delta a_\mu^{2L} = a_\mu^B + a_\mu^F. \quad (4.2)$$

The pseudoscalar  $A$  and the charged Higgs boson  $H^\pm$  can also contribute to  $a_\mu^F$  and  $a_\mu^B$  via loop effects, with their contributions decreasing as their masses increase [100]. The dominant contribution to  $\Delta a_\mu$  comes from  $a_\mu^B$ , which consists of three parts and have

$$a_\mu^B = a_\mu^{\text{EW}} + a_\mu^{\text{Yuk}} + a_\mu^{\text{non-Yuk}}. \quad (4.3)$$

The component  $a_\mu^{\text{EW}}$  corresponds to contributions from the SM-like Higgs,  $a_\mu^{\text{non-Yuk}}$  represents QCD contributions without new Yukawa couplings and  $a_\mu^{\text{Yuk}}$  accounts for QCD contributions with new Yukawa couplings. The latter has the form

$$a_\mu^{\text{Yuk}} = \frac{\alpha_{em}^2 m_\mu^2}{574\pi^2 c_W^4 s_W^4 m_Z^4} \left[ a_{0,0}^0 + a_{5,0}^0 \Lambda_5 + (a_{0,0}^1 \frac{\tan^2 \beta - 1}{\tan \beta} + a_{5,0}^1 \frac{\tan^2 \beta - 1}{\tan \beta} \Lambda_5) \cos(\beta - \alpha) \right], \quad (4.4)$$

where  $\Lambda_5$  is defined as  $2m_{12}^2/v^2 \sin \beta \cos \beta$ , and the coefficients  $a_{0,0}^0$ ,  $a_{0,0}^1$ ,  $a_{5,0}^0$ , and  $a_{5,0}^1$  are given in the Appendix of Ref. [100]. In our analysis,  $m_{12}^2$  is significantly larger than both  $\tan \beta$  and  $v^2$ , causing  $a_\mu^{\text{Yuk}}$  to be nearly proportional to  $m_{12}^2$ . Consequently,  $\Delta a_\mu$  increases with increasing  $m_{12}^2$ .

In Fig. 2, the surviving samples are shown in the  $\tan \beta$  versus  $\alpha$  (upper three, lower left, and lower middle) and  $\mu_{\gamma\gamma}$  versus  $\alpha$  (lower right) planes. The color coding indicates the following observables: the cross section  $\sigma(gg \rightarrow h)$  (upper left), the branching ratio  $\text{Br}(h \rightarrow \gamma\gamma)$  (upper middle), the cross section  $\sigma(gg \rightarrow h \rightarrow \gamma\gamma)$  (upper right and lower right), the squared reduced top-Higgs coupling  $(C_{tth}/C_{tth}^{\text{SM}})^2$  normalized to its SM value

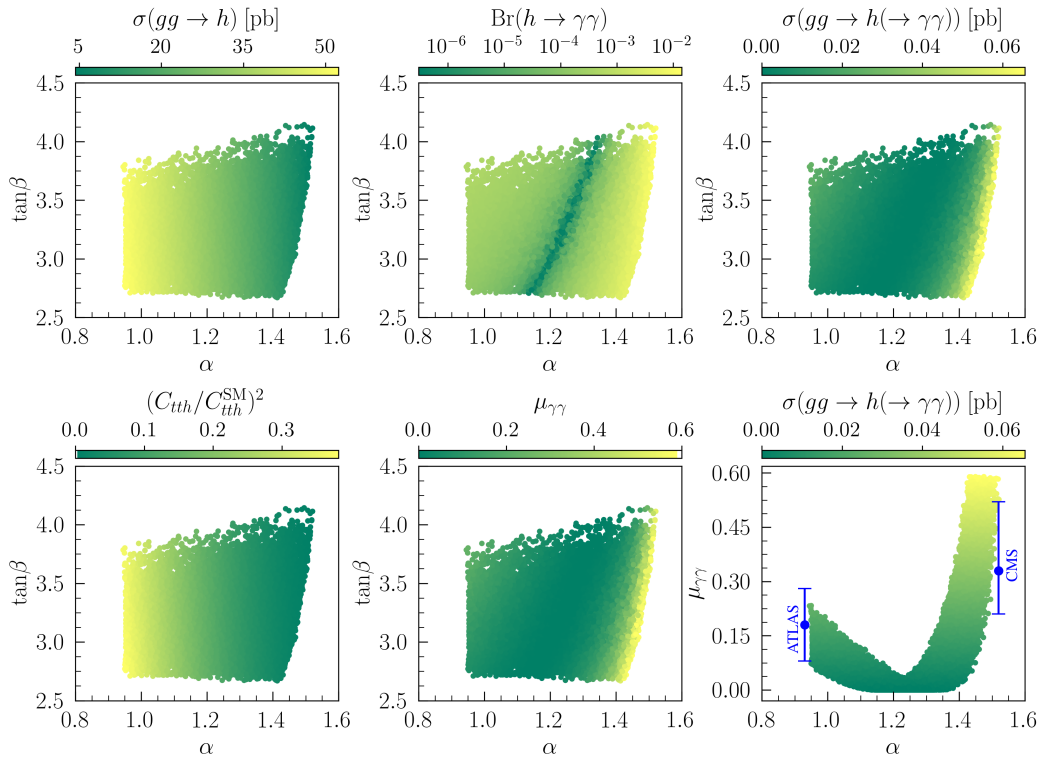


**Figure 2.** Surviving samples in the  $\tan\beta$  versus  $\alpha$  (upper three, lower left, and lower middle) and  $\mu_{\gamma\gamma}$  versus  $\alpha$  (lower right) planes. Colors indicate the following observables: the cross section  $\sigma(gg \rightarrow h)$  (upper left), the branching ratio  $\text{Br}(h \rightarrow \gamma\gamma)$  (upper middle), the cross section  $\sigma(gg \rightarrow h \rightarrow \gamma\gamma)$  (upper right and lower right), the reduced top-Higgs coupling  $(C_{tth}/C_{tth}^{\text{SM}})^2$  normalized to the SM value in the 2HDM-I (lower left), and the diphoton signal strength  $\mu_{\gamma\gamma}$  (lower middle). In the lower right panel, markers represent the measured signal strengths and uncertainties for the 95 GeV diphoton excess reported by CMS [8] and ATLAS [7].

in the 2HDM-I (lower left), and the diphoton signal strength  $\mu_{\gamma\gamma}$  (lower middle). The measured signal strength and associated uncertainties for the 95 GeV diphoton excess observed by CMS and ATLAS are also indicated in the lower right panel of Fig. 2. The signal strength  $\mu_{\gamma\gamma}$  is a well-known observable for probing BSM phenomenology in the diphoton channel. It can be parameterized as

$$\mu_{\gamma\gamma}(h_{95}) = \frac{\sigma_{\text{BSM}}(gg \rightarrow h_{95}) \times \text{Br}_{\text{BSM}}(h_{95} \rightarrow \gamma\gamma)}{\sigma_{\text{SM}}(gg \rightarrow h_{95}) \times \text{Br}_{\text{SM}}(h_{95} \rightarrow \gamma\gamma)}, \quad (4.5)$$

where  $\sigma_{\text{BSM}}(gg \rightarrow h_{95})$  ( $\sigma_{\text{SM}}(gg \rightarrow h_{95})$ ) denotes the production cross section of the light Higgs  $h_{95}$  in the BSM (SM), and  $\text{Br}_{\text{BSM}}(h_{95} \rightarrow \gamma\gamma)$  ( $\text{Br}_{\text{SM}}(h_{95} \rightarrow \gamma\gamma)$ ) is the corresponding diphoton branching ratio. In the SM, the cross section for  $gg \rightarrow h_{95}$  at the 14 TeV LHC is 79.83 pb [103], and the branching ratio for  $h_{95} \rightarrow \gamma\gamma$  is  $1.39 \times 10^{-3}$  [104]. The measured diphoton signal strengths are  $\mu_{\gamma\gamma}^{\text{ATLAS}} = 0.18^{+0.1}_{-0.1}$  from ATLAS [7] and  $\mu_{\gamma\gamma}^{\text{CMS}} = 0.33^{+0.19}_{-0.12}$  from CMS [8]. Several conclusions can be drawn from Fig. 2:

- From the upper left and lower left panels of Fig. 2, one can observe that both the cross section  $\sigma(gg \rightarrow h)$  and the reduced top-Higgs coupling  $(C_{tth}/C_{tth}^{\text{SM}})^2$  exhibit

similar trends with respect to  $\alpha$  and  $\tan\beta$ . They are approximately proportional to  $\cos^2\alpha$  and inversely proportional to  $\sin^2\beta$ . This behavior of the reduced top-Higgs coupling is consistent with Eq. (2.7). In the 2HDM-I, the cross section  $\sigma(gg \rightarrow h)$  can be obtained by rescaling the SM prediction by a factor of  $\cos^2\alpha/\sin^2\beta$ , assuming that the loop contribution is dominated by the top quark, which is typically the case.

- From the upper middle panel of Fig. 2, it is evident that the branching ratio of the lighter Higgs boson decaying into diphoton,  $\text{Br}(h \rightarrow \gamma\gamma)$ , primarily depends on the parameters  $\alpha$  and  $\tan\beta$ . The branching ratio reaches its maximum value of approximately  $10^{-2}$  with  $\alpha \approx 1.5$ , which corresponds to  $\sin(\beta - \alpha) \approx -0.2$ , and reaches its minimum value of about  $10^{-6}$  when  $\alpha \approx 1.25$ , which corresponds to  $\sin(\beta - \alpha) \approx 0$ . This behavior can be understood from the partial decay width  $\Gamma(h \rightarrow \gamma\gamma)$ , which is described by Eq. (2.8), where the loop functions take typical values  $A_0(\tau_{H^\pm}) \approx 0.34$ ,  $A_{1/2}(\tau_f) \approx 1.4$ , and  $A_1(\tau_W) \approx -7.6$  in our parameter scan. The dominant contribution to  $\Gamma(h \rightarrow \gamma\gamma)$  arises from the  $W$  boson loop. When  $\sin(\beta - \alpha)$  approaches zero, the coupling of  $h$  to the  $W$  boson becomes suppressed (see Eq. (2.6)), leading to a negligible  $W$  contribution to the diphoton decay width.
- From the upper right and lower middle panels of Fig. 2, it can be seen that the cross section  $\sigma(gg \rightarrow h \rightarrow \gamma\gamma)$  reaches up to 0.065 pb around  $\sin(\beta - \alpha) \approx -0.2$ , corresponding to a diphoton signal strength of  $\mu_{\gamma\gamma} \approx 0.59$ . The 95 GeV diphoton excess observed by CMS and ATLAS can be accommodated within the  $1\sigma$  range for parameter points with  $\alpha \approx 1.5$  and  $\alpha \approx 0.95$ , corresponding to  $\sin(\beta - \alpha) \approx -0.2$  and  $\sin(\beta - \alpha) \approx 0.35$  respectively, as shown in the lower right panel of Fig. 2.

In Fig. 3, we present the surviving samples in the  $\tan\beta$  versus  $\alpha$  plane, with color indicating the cross section  $\sigma(pp \rightarrow t\bar{t}h \rightarrow \gamma\gamma)$  at the 14 TeV High-Luminosity LHC (HL-LHC) (left), the 27 TeV High-Energy LHC (HE-LHC) (middle), and the 100 TeV Future Circular Collider (FCC-hh) (right). The cross section  $\sigma(pp \rightarrow t\bar{t}h \rightarrow \gamma\gamma)$  at the HL-LHC is calculated as

$$\sigma(pp \rightarrow t\bar{t}(h \rightarrow \gamma\gamma)) = |\sigma(pp \rightarrow t\bar{t}H)|_{m_h=95\text{GeV}}^{\text{SM}} \times (C_{t\bar{t}h}^2/C_{t\bar{t}h}^{\text{SM}})^2 \times \text{Br}(h \rightarrow \gamma\gamma), \quad (4.6)$$

where  $|\sigma(pp \rightarrow t\bar{t}H)|_{m_h=95\text{GeV}}^{\text{SM}}$  is the SM cross section for the process  $pp \rightarrow t\bar{t}H$  with a Higgs mass of 95 GeV. The value at next-to-leading order (NLO) is reported to be 1268 fb, as given in Ref. [103]. The cross sections at the HE-LHC and FCC-hh are calculated using the following rescaling formula:

$$\sigma_{\text{HE-LHC(FCC-hh)}} = \sigma_{\text{HE-LHC(FCC-hh)}}^{\text{P1}} \times \frac{C_{t\bar{t}h}^2 \times \text{Br}(h \rightarrow \gamma\gamma)}{(C_{t\bar{t}h}^{\text{P1}})^2 \times \text{Br}^{\text{P1}}(h \rightarrow \gamma\gamma)}, \quad (4.7)$$

where  $\sigma_{\text{HE-LHC}}^{\text{P1}}$  and  $\sigma_{\text{FCC-hh}}^{\text{P1}}$  are cross sections for the Benchmark Point P1 at the 27 TeV HE-LHC and 100 TeV FCC-hh, calculated using MadGraph5\_aMC@NLO\_v3.4.2 [105, 106], and they correspond to 0.64 fb and 7.75 fb, respectively. Additionally,  $C_{t\bar{t}h}^{\text{P1}}$  and  $\text{Br}^{\text{P1}}(h \rightarrow \gamma\gamma)$  denote the reduced coupling and the branching ratio for this benchmark point. For

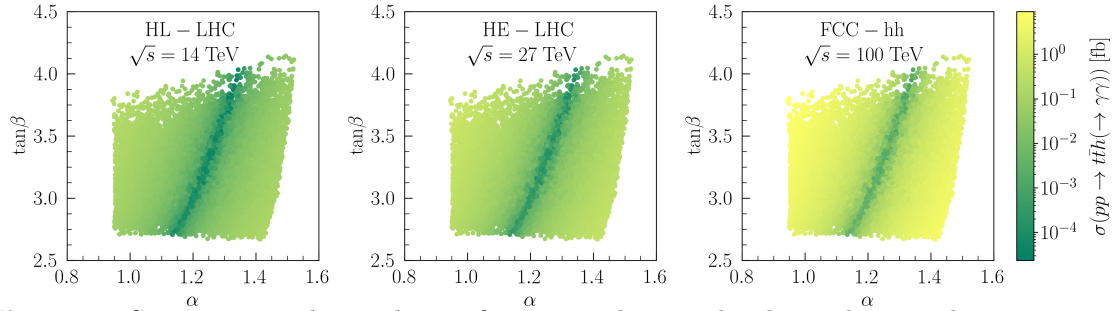


**Figure 3.** Surviving samples on the  $\tan\beta$  versus  $\alpha$  plane, with colors indicating the cross section  $\sigma(pp \rightarrow t\bar{t}h(\rightarrow \gamma\gamma))$  at 14 TeV High-Luminosity LHC (HL-LHC) (left), 27 TeV High-Energy LHC (HE-LHC) (middle), and 100 TeV Future Circular Collider (FCC-hh) (right).

**Table 1.** The detailed information of five benchmark points for surviving samples.

	P1	P2	P3	P4	P5
$\alpha$	0.963	1.42	1.44	1.41	1.46
$\tan\beta$	3.70	3.13	3.50	2.94	3.35
$m_{H^\pm}(m_A)$ [GeV]	167	176	196	224	167
$m_{12}$ [GeV]	2835	3530	3544	3890	3047
$\lambda_1$	2.63	1.80	2.348	1.64	1.96
$\lambda_2$	0.126	0.151	0.148	0.155	0.148
$\lambda_3$	1.31	1.28	1.54	1.92	1.14
$\lambda_4$	-0.65	-0.71	-0.85	-1.03	-0.641
$\lambda_5$	-0.65	-0.71	-0.85	-1.03	-0.641
T [ $\times 10^{-2}$ ]	-1.5	-1.7	-1.7	-1.7	-1.67
S [ $\times 10^{-2}$ ]	1.0	1.1	0.98	0.82	1.18
U [ $\times 10^{-4}$ ]	-3.9	-5.1	-5.8	-6.5	-4.6
$\text{Br}(h \rightarrow \gamma\gamma)$ [ $\times 10^{-3}$ ]	0.45	2	2.6	2.6	3.6
$\sigma(gg \rightarrow h)$ [pb]	50	13	11	14	10
$\sigma(gg \rightarrow h(\rightarrow \gamma\gamma))$ [fb]	22.5	26	28.6	36.4	36
$\mu_{\gamma\gamma}$	0.20	0.24	0.26	0.33	0.33
$(C_{h\bar{t}t}/C_{h\bar{t}t}^{\text{SM}})^2$	0.348	0.025	0.017	0.029	0.014
$\sigma(pp \rightarrow t\bar{t}h(\rightarrow \gamma\gamma))$ [fb]	0.20	0.063	0.056	0.095	0.064
$\chi^2$	91.2	92.9	92.3	93.1	92.4
P-value	0.86	0.83	0.84	0.83	0.84
$\text{Br}(B \rightarrow X_s \gamma)$ [ $\times 10^{-4}$ ]	3.08	3.04	3.07	3.04	3.05
$\text{Br}(B_d \rightarrow \mu^+ \mu^-)$ [ $\times 10^{-10}$ ]	0.99	1.0	0.98	1.0	1.0
$\text{Br}(B_s \rightarrow \mu^+ \mu^-)$ [ $\times 10^{-9}$ ]	3.11	3.14	3.09	3.13	3.14
$\Delta a_\mu$ [ $\times 10^{-9}$ ]	2.15	2.72	2.57	2.25	2.30

the surviving samples, the maximum cross sections of the process  $pp \rightarrow t\bar{t}(h \rightarrow \gamma\gamma)$  can reach 0.23 fb at the HL-LHC, 0.75 fb at the HE-LHC, and 9.07 fb at the FCC-hh. Detailed information on five representative benchmark points selected from the surviving samples is provided in Table 1.

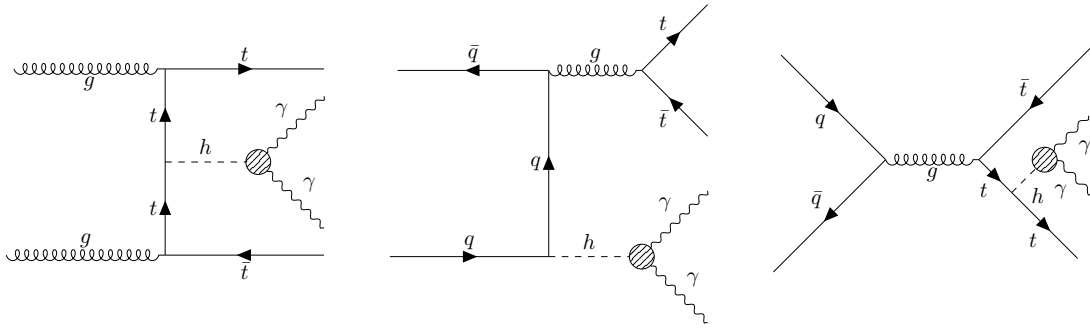


**Figure 4.** Main Feynman Diagrams for the Process  $pp \rightarrow t\bar{t}h(\rightarrow \gamma\gamma)$  at Leading Order (LO) in 2HDM-I.

## 5 Future collider simulations and discussion

In this study, we focus on the process  $pp \rightarrow t(\rightarrow W^+b)\bar{t}(\rightarrow W^-b)h(\rightarrow \gamma\gamma)$ , where the Higgs boson  $h$  is produced in association with a top-quark pair and subsequently decays into two photons. Each top quark decays into a  $W$  boson and a  $b$  quark. The leading-order (LO) Feynman diagrams for the process  $pp \rightarrow t\bar{t}h(\rightarrow \gamma\gamma)$  in the 2HDM-I are shown in Fig. 4. The decay of  $h$  into a diphoton proceeds only via loop processes, which significantly suppresses the corresponding cross section. Nevertheless, the diphoton final state offers a relatively clean experimental signature at hadron colliders. In particular, the invariant mass of the diphoton system gives rise to a narrow resonance peak around the mass of  $h$ , making the signal easier to isolate. Moreover, the presence of the associated top-quark pair further suppresses SM backgrounds, as the top quark decays into a  $W$  boson and a  $b$  quark, leaving additional detectable jets in the final state. In addition, the  $W$  boson can decay leptonically, producing a charged lepton and a neutrino; the latter escapes detection and contributes to missing transverse momentum, while the charged lepton provides a useful trigger for event selection.

On the other hand, the process  $Z \rightarrow e^+e^-$  should also be considered, as the two electrons may be misidentified as photons. This process has a relatively large production cross section. However, when associated with top-quark pair production, the cross section of  $pp \rightarrow t\bar{t}Z(\rightarrow e^+e^-)$  is significantly reduced, reaching a level comparable to that of the signal. Moreover, the probability for an electron to be misidentified as a photon is typically below 0.1 [107], indicating that this background is negligible in the present analysis. Similarly, jets can also be misidentified as photons, but the corresponding misidentification rate is usually very low, ranging from  $10^{-3}$  to  $10^{-5}$  [108]. Therefore, these reducible backgrounds are not considered further in this study.

The SM backgrounds can be categorized into two types: resonant and non-resonant. For the resonant backgrounds, we consider the processes  $t\bar{t}H$  and  $tjH$ , where  $H$  denotes the 125 GeV SM-like Higgs boson. These correspond to the following decay chains:

$$pp \rightarrow t(\rightarrow W^+b)\bar{t}(\rightarrow W^-b)H(\rightarrow \gamma\gamma), \quad \text{and} \quad pp \rightarrow t(\rightarrow W^+b)jH(\rightarrow \gamma\gamma), \quad (5.1)$$

respectively. For the non-resonant backgrounds, we include the processes  $t\bar{t}\gamma\gamma$ ,  $b\bar{b}\gamma\gamma$ ,  $tj\gamma\gamma$ ,  $t\bar{t}\gamma$ , and  $Wjj\gamma\gamma$ , corresponding to:

$$\begin{aligned}
pp &\rightarrow t(\rightarrow W^+b)\bar{t}(\rightarrow W^-\bar{b})\gamma\gamma, & pp &\rightarrow b\bar{b}\gamma\gamma, \\
pp &\rightarrow t(\rightarrow W^+b)j\gamma\gamma, & pp &\rightarrow t(\rightarrow W^+b)\bar{t}(\rightarrow W^-\bar{b})\gamma, \\
pp &\rightarrow W(\rightarrow \ell\nu)jj\gamma\gamma.
\end{aligned} \tag{5.2}$$

Monte Carlo simulations for both signal and background processes are performed using the `MadGraph5_aMC@NLO_v3.4.2` package [105, 106]. In the collider simulation, parton distribution functions (PDFs) are set to `NNPDF23LO1` via `LHAPDF6` [109, 110]. Particle decays, parton showering, and hadronization are handled by `PYTHIA_v8.2` [111], interfaced through the `MG5a-MC-PY8-interface`. Jet clustering is performed using the anti- $k_T$  algorithm [112]. Detector effects are simulated with `Delphes-3.5.0` [113, 114]. The final analysis of the simulated events is carried out using `MadAnalysis5 v1.9.60` [115].

Monte Carlo simulations are performed at the 14 TeV HL-LHC, the 27 TeV HE-LHC [116], and the 100 TeV FCC-hh [117], which are designed to deliver integrated luminosities of  $3 \text{ ab}^{-1}$ ,  $10 \text{ ab}^{-1}$ , and  $30 \text{ ab}^{-1}$ , respectively. In Fig. 5, the normalized distributions of several kinematic observables for the signal and SM backgrounds at the 14 TeV HL-LHC are shown, including:  $\Delta R[j_1, j_2]$  (upper left), the jet multiplicity  $N[j]$  (upper middle), the transverse momenta of the leading jet  $p_T^{j_1}$  (upper right), the leading lepton  $p_T^{\ell_1}$  (middle left), the leading and subleading photons  $p_T^{\gamma_1}$  (middle middle) and  $p_T^{\gamma_2}$  (middle right), the transverse mass  $M_T[\gamma_1\gamma_2]$  (lower left), the invariant mass  $M[\gamma_1\gamma_2]$  (lower middle), and  $M[\gamma_1\gamma_2b]$  (lower right). In each case,  $\gamma_1$  denotes the photon with the highest energy,  $\gamma_2$  the next highest, and similarly for  $j_1$  and  $j_2$ . Here, the invariant mass  $M[\gamma_1\gamma_2]$  is defined as

$$M[\gamma_1\gamma_2] \equiv \sqrt{(p_0^{\gamma_1} + p_0^{\gamma_2})^2 - (p_1^{\gamma_1} + p_1^{\gamma_2})^2 - (p_2^{\gamma_1} + p_2^{\gamma_2})^2 - (p_3^{\gamma_1} + p_3^{\gamma_2})^2}, \tag{5.3}$$

and the transverse masses  $M_T[\gamma_1\gamma_2]$  is defined as

$$M_T[\gamma_1\gamma_2] \equiv \sqrt{(p_0^{\gamma_1} + p_0^{\gamma_2})^2 - (p_1^{\gamma_1} + p_1^{\gamma_2})^2 - (p_2^{\gamma_1} + p_2^{\gamma_2})^2}. \tag{5.4}$$

The definition of the invariant mass  $M[\gamma_1\gamma_2b]$  follows the same form as that of  $M[\gamma_1\gamma_2]$ , with the inclusion of the four-momentum of the  $b$ -jet. From this figure, one can notice the following details:

- From the upper left panel of Fig. 5, one can see that the backgrounds of  $tjH$  and  $tj\gamma\gamma$  have more events clustered at larger  $\Delta R[j_1, j_2]$  values compared to the signal. Thus, choosing an appropriate  $\Delta R[j_1, j_2]$  can effectively reduce these backgrounds.
- The upper middle panel of Fig. 5 shows that the  $b\bar{b}\gamma\gamma$  background typically has fewer jets than others. By choosing a higher jet count threshold,  $N[j]$ , one can significantly reduce this background.

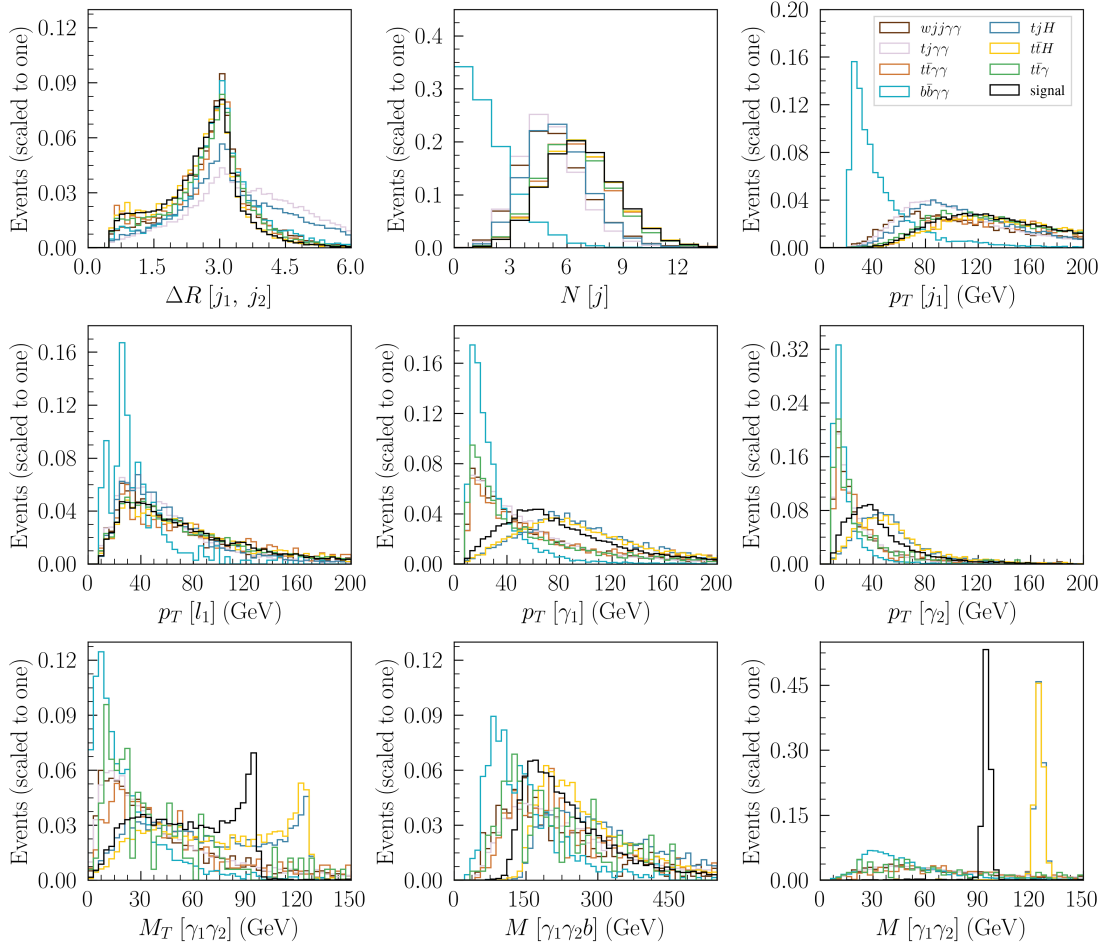


**Figure 5.** The normalized distributions of  $\Delta R[j_1, j_2]$  (upper left),  $N[j]$  (upper middle),  $p_T^{j_1}$  (upper right),  $p_T^{l_1}$  (upper middle),  $p_T^{\gamma_1}$  (middle),  $p_T^{\gamma_2}$  (middle right),  $M_T[\gamma_1\gamma_2]$  (lower left),  $M[\gamma_1\gamma_2]$  (lower middle) and  $M[\gamma_1\gamma_2 b]$  (lower right) for the signal and SM backgrounds at 14 TeV HL-LHC.

- The upper right, middle, and middle right panels of Fig. 5 show that the non-resonant backgrounds, especially  $b\bar{b}\gamma\gamma$ , typically have lower transverse momenta for  $j_1$ ,  $\gamma_1$ , and  $\gamma_2$ . Consequently, choosing higher transverse momentum thresholds for these particles can effectively suppress the non-resonant background.
- From the lower left panel of Fig. 5, one can observe that the transverse mass  $M_T[\gamma_1\gamma_2]$  for non-resonant backgrounds tends to be distributed at lower values. In contrast, the distributions for the signal and resonant backgrounds peak at higher values and exhibit sharp cutoffs near their respective resonance masses, i.e., 95 GeV for the signal and 125 GeV for the SM-like Higgs.
- From the lower middle panel of Fig. 5, one can observe that both the resonant background and the signal show a preference for a larger invariant mass of  $\gamma_1$ ,  $\gamma_2$ , and  $b$ . Consequently, choosing a higher  $M[\gamma_1\gamma_2 b]$  can effectively reduce the non-resonant

background.

- From the lower middle panel of Fig. 5, one can observe that the invariant mass  $M[\gamma_1\gamma_2]$  distributions for the signal and resonant backgrounds exhibit narrow peaks centered around their respective resonance masses, i.e., 95 GeV for the signal and 125 GeV for the SM-like Higgs. In contrast, the non-resonant backgrounds show broader distributions with lower invariant mass values and lack any distinct peak structure.

The events selected for analysis are required to satisfy the following basic kinematic criteria for leptons, jets, and photons:

$$p_T^{j/b} > 20 \text{ GeV}, p_T^{\ell/\gamma} > 10 \text{ GeV}, |\eta_i| < 5, \Delta R[i, j] > 0.4. \quad (i, j = j, b, \ell, \gamma) \quad (5.5)$$

In addition, at least one  $W$  boson from the top quark decays is required to decay leptonically (i.e., into a lepton and a neutrino), which helps suppress the  $b\bar{b}\gamma\gamma$  background. Furthermore, two isolated photons are required in the final state to allow for invariant mass reconstruction. Based on the distributions shown in Fig. 5, the following selection cuts are applied in the Monte Carlo simulations for the HL-LHC:

- **Basic Cut:** We select events containing at least one lepton ( $N(\ell) \geq 1$ ), two photons ( $N(\gamma) \geq 2$ ), two jets ( $N(j) \geq 2$ ), and at least one b-jet ( $N(b) \geq 1$ ). For the transverse momentum ( $p_T$ ) of jets and photons, the following requirements apply:

$$p_T[\gamma_1] > 30 \text{ GeV}, p_T[j_1] > 40 \text{ GeV}, p_T[j_2] < 220 \text{ GeV}. \quad (5.6)$$

The spatial separation between jets and photons should satisfy the following criteria:

$$\Delta R[j_1, j_2] < 4, \Delta R[\gamma_1, \gamma_2] < 3.6. \quad (5.7)$$

To further suppress the background from  $t\bar{t}\gamma$ , we require that the phase angle of the b-jet ( $\theta_{b_1}$ ), the pseudorapidity of the jet and lepton ( $\eta_{j_1}$  and  $\eta_{\ell_1}$ ), and the Lorentz factor of the jet ( $\gamma_{j_1}$ ) meet the following conditions:

$$0.2 < \theta_{b_1} < 3, \eta_{j_1} > -2.6, \eta_{\ell_1} > -2.5, \gamma_{j_1} < 50. \quad (5.8)$$

- **Mass Cut:** For the invariant masses of the diphoton pair ( $M[\gamma_1\gamma_2]$ ) and the photon with jet ( $M[\gamma_2j_1]$ ), we choose:

$$92 \text{ GeV} < M[\gamma_1\gamma_2] < 98 \text{ GeV}, M[\gamma_2j_1] < 390 \text{ GeV}. \quad (5.9)$$

For the transverse masses of the photon, diphoton, and diphoton with a b-jet ( $M_T[\gamma_1]$ ,  $M_T[\gamma_1\gamma_2]$ , and  $M_T[\gamma_1\gamma_2b_1]$ ), we select:

$$M_T[\gamma_1] < 300 \text{ GeV}, M_T[\gamma_1\gamma_2] < 96 \text{ GeV}, M_T[\gamma_1\gamma_2b_1] < 440 \text{ GeV}. \quad (5.10)$$

- **Energy Cut:** The transverse energy ( $E_T$ ), transverse hadronic energy ( $H_T$ ), missing transverse energy ( $\cancel{E}_T$ ), and missing transverse hadronic energy ( $\cancel{H}_T$ ) should meet the following criteria:

$$E_T > 200 \text{ GeV}, H_T < 900 \text{ GeV}, 10\text{GeV} < \cancel{E}_T < 190 \text{ GeV}, \cancel{H}_T > 30 \text{ GeV}. \quad (5.11)$$

**Table 2.** Cut flow of cross sections at the 14 TeV HL-LHC for benchmark point P1 with an integrated luminosity of  $L = 300 \text{ fb}^{-1}$ , as detailed in Table 1.

Cuts	Signal( $\sigma \times L$ )	Background( $\sigma \times L$ )						
	$t\bar{t}h$	$t\bar{t}\gamma$	$t\bar{t}H$	$tjH$	$b\bar{b}\gamma\gamma$	$t\bar{t}\gamma\gamma$	$tj\gamma\gamma$	$Wjj\gamma\gamma$
Initial	60	1536000	168	23	2293800	3354	5253	65400
Basic cut	5.27	4577.3	17.25	0.712	848.7	200.0	89.61	268.1
Mass cut	4.13	46.08	0.029	0.0	0.0	6.47	2.67	4.58
Energy cut	3.76	0.0	0.029	0.0	0.0	5.8	1.91	3.27

**Table 3.** Cut flow of the cross sections at 27 TeV HE-LHC for benchmark point P1 with an integrated luminosity of  $L = 300 \text{ fb}^{-1}$ , as detailed in Table 1.

Cuts	Signal( $\sigma \times L$ )	Background( $\sigma \times L$ )						
	$t\bar{t}h$	$t\bar{t}\gamma$	$t\bar{t}H$	$tjH$	$b\bar{b}\gamma\gamma$	$t\bar{t}\gamma\gamma$	$tj\gamma\gamma$	$Wjj\gamma\gamma$
Initial	192	3168000	927	115	3408000	14178	19920	206009
Basic cut	13.92	6874.6	80.06	3.23	1192.8	776.6	358.5	995.0
Mass cut	9.14	0.0	0.111	0.002	68.16	17.22	5.13	12.36
Energy cut	8.59	0.0	0.111	0.002	0.0	16.27	3.21	10.3

**Table 4.** Cut flow of the cross sections at 100 TeV FCC-hh for benchmark point P1 with an integrated luminosity of  $L = 300 \text{ fb}^{-1}$ , as detailed in Table 1.

Cuts	Signal( $\sigma \times L$ )	Background( $\sigma \times L$ )						
	$t\bar{t}h$	$t\bar{t}\gamma$	$t\bar{t}H$	$tjH$	$b\bar{b}\gamma\gamma$	$t\bar{t}\gamma\gamma$	$tj\gamma\gamma$	$Wjj\gamma\gamma$
Initial	2325	33120000	11724	1005	14856000	141570	138120	1255800
Basic cut	101.42	53985	621	17.1	6388.1	4764.2	1446.7	4897.6
Mass cut	64.94	662.4	1.06	0.0	148.6	91.0	24.82	37.67
Energy cut	59.75	0.0	0.821	0.0	0.0	78.86	21.28	25.12

These cuts are performed on both our reference points and background events to calculate the signal significance. The results of these sequential cuts are detailed in Table 2, where the integrated luminosity is set to  $300 \text{ fb}^{-1}$ . The dominant backgrounds,  $Wjj\gamma\gamma$ ,  $b\bar{b}\gamma\gamma$ , and  $t\bar{t}\gamma$ , are significantly reduced by more than two to three orders of magnitude after the base cut, while the signal reduction is limited to one order of magnitude. Subsequent cuts at the invariant mass and transverse mass effectively preserved the signal while further reducing the background. After these cuts,  $t\bar{t}\gamma$ ,  $t\bar{t}\gamma\gamma$ ,  $tj\gamma\gamma$ , and  $Wjj\gamma\gamma$  showed reductions of more than an order of magnitude, while  $t\bar{t}H$ ,  $tjH$ , and  $b\bar{b}\gamma\gamma$  were nearly eliminated. The final cut on transverse energy and transverse hadronic energy additionally minimized the  $t\bar{t}\gamma$  background to negligible levels. In the end, only minimal instances of  $t\bar{t}H$ ,  $t\bar{t}\gamma\gamma$ ,  $tj\gamma\gamma$ , and  $Wjj\gamma\gamma$  remained.

The distributions of various kinematic variables for the signal and SM backgrounds at the 27 TeV HE-LHC and the 100 TeV FCC-hh have been examined and found to be similar to those at the HL-LHC, as shown in Fig. 5. In contrast to the Monte Carlo simulations for the HL-LHC, the following selection cuts are applied in the simulations for the HE-LHC:

- **Basic Cut:** We select events that include at least one lepton ( $N(\ell) \geq 1$ ), two photons ( $N(\gamma) \geq 2$ ), two jets ( $N(j) \geq 2$ ), and at least one b-jet ( $N(b) \geq 1$ ). For the transverse

momentum ( $p_T$ ) of jets, leptons, and photons, the following cuts are applied:

$$p_T[j_1] > 30 \text{ GeV}, p_T[\ell_1] > 20 \text{ GeV}, p_T[\gamma_1] > 30 \text{ GeV}. \quad (5.12)$$

The spatial separation between jets and photons should meet the following criteria:

$$\Delta R[j_1, j_2] < 4, \Delta R[\gamma_1, \gamma_2] < 3.4. \quad (5.13)$$

To further reduce the background from  $t\bar{t}\gamma$ , the pseudorapidity of the jet and lepton ( $\eta_{j_1}$  and  $\eta_{\ell_1}$ ) should meet the following criteria:

$$\eta_{j_1} > -3.4, \eta_{\ell_1} < 3.5. \quad (5.14)$$

- **Mass Cut:** For the invariant masses of the diphoton pair ( $M[\gamma_1\gamma_2]$ ) and the diphoton with a b-jet ( $M[\gamma_1\gamma_2b_1]$ ), we require:

$$93 \text{ GeV} < M[\gamma_1\gamma_2] < 97 \text{ GeV}, M[\gamma_1\gamma_2b_1] > 120 \text{ GeV}. \quad (5.15)$$

For the transverse masses of the lepton, photon, diphoton, and diphoton with a b-jet ( $M_T[\ell_1]$ ,  $M_T[\gamma_1]$ ,  $M_T[\gamma_1\gamma_2]$ , and  $M_T[\gamma_1\gamma_2b_1]$ ), we require:

$$M_T[\ell_1] < 40 \text{ GeV}, M_T[\gamma_1] < 380 \text{ GeV}, M_T[\gamma_1\gamma_2b] > 6 \text{ GeV}, M_T[\gamma_1\gamma_2b_1] < 500 \text{ GeV}. \quad (5.16)$$

- **Energy Cut:** The missing transverse energy ( $\cancel{E}_T$ ) is used to reduce the background of  $Wjj\gamma\gamma$ , which require

$$\cancel{E}_T > 15 \text{ GeV}. \quad (5.17)$$

The cut flow for signal and background at the HE-LHC with an integrated luminosity of  $L = 300 \text{ fb}^{-1}$  is shown in Table 3. The backgrounds of  $t\bar{t}\gamma$ ,  $b\bar{b}\gamma\gamma$  and  $Wjj\gamma\gamma$  still play an important role. After the basic cut, the backgrounds of  $t\bar{t}\gamma$  and  $b\bar{b}\gamma\gamma$  are reduced by over two and three orders of magnitude, respectively. These backgrounds are further suppressed by subsequent cuts at the invariant mass and transverse mass. The  $t\bar{t}\gamma$  background is nearly eliminated and no longer dominant. The  $t\bar{t}H$  and  $tjH$  backgrounds become nearly negligible. Finally, the missing transverse energy cut effectively eliminates the  $b\bar{b}\gamma\gamma$  background. However, the  $t\bar{t}\gamma\gamma$ ,  $tj\gamma\gamma$ , and  $Wjj\gamma\gamma$  backgrounds are difficult to remove and ultimately persist.

The following selection cuts are applied in the FCC-hh simulations:

- **Basic Cut:** We select events containing at least one lepton ( $N(\ell) \geq 1$ ), two photons ( $N(\gamma) \geq 2$ ), two jets ( $N(j) \geq 2$ ), and at least one b-jet ( $N(b) \geq 1$ ). For the transverse momentum ( $p_T$ ) of the jets and photons, we have the following requirements

$$p_T[\gamma_1] > 35 \text{ GeV}, p_T[j_2] < 220 \text{ GeV}, p_T[b_1] > 25 \text{ GeV}. \quad (5.18)$$

The spatial separation between jets and photons should meet the following criteria:

$$\Delta R[j_1, j_2] < 4, \Delta R[\gamma_1, \gamma_2] < 3.4. \quad (5.19)$$

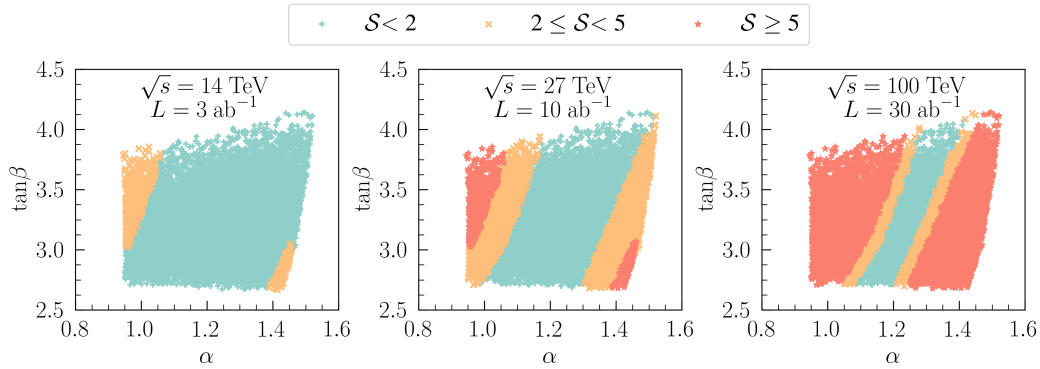


**Figure 6.** Statistical significance of surviving samples in the  $\tan\beta$  versus  $\alpha$  planes at the 14 TeV HL-LHC for integrated luminosities of  $L = 3 \text{ ab}^{-1}$  (left), the 27 TeV HE-LHC for integrated luminosities of  $L = 10 \text{ ab}^{-1}$  (middle), and the 100 TeV FCC-hh for  $L = 30 \text{ ab}^{-1}$  (right).

To further reduce the background from  $t\bar{t}\gamma$ , we require that the phase angle of the lepton ( $\theta_{\ell_1}$ ) and the pseudorapidity of the jet ( $\eta_{j_1}$ ) meet the following criteria:

$$\theta_{\ell_1} > 0.1, \quad \eta_{j_1} > -3.8. \quad (5.20)$$

- **Mass Cut:** For the invariant mass of the diphoton pair  $M[\gamma_1\gamma_2]$ , we choose the following criteria:

$$93 \text{ GeV} < M[\gamma_1\gamma_2] < 97 \text{ GeV}. \quad (5.21)$$

For the transverse mass of the photon and lepton, we apply the following criteria:

$$M_T[\gamma_1] < 330 \text{ GeV}, \quad M_T[\ell_1] < 295 \text{ GeV}. \quad (5.22)$$

- **Energy Cut:** The transverse hadronic energy ( $H_T$ ) and the missing transverse energy ( $\cancel{E}_T$ ) should meet the following criteria:

$$150 \text{ GeV} < H_T < 900 \text{ GeV}, \quad \cancel{E}_T > 10 \text{ GeV}. \quad (5.23)$$

The cut flow of the cross sections for signal and background at the FCC-hh with an integrated luminosity of  $L = 300 \text{ fb}^{-1}$  is shown in Table 4. As the collision energy increases from 27 to 100 TeV, the cross sections for all signals and backgrounds, except for the  $b\bar{b}\gamma\gamma$  background, increase about ten times. The primary backgrounds are  $t\bar{t}\gamma$ ,  $b\bar{b}\gamma\gamma$ , and  $Wjj\gamma\gamma$ . The basic cut significantly reduces these backgrounds to a rare occurrence. After the basic cut, the backgrounds  $b\bar{b}\gamma\gamma$ ,  $t\bar{t}\gamma\gamma$ ,  $tj\gamma\gamma$ , and  $Wjj\gamma\gamma$  become equally significant, each retaining a few thousand events. The resonance background  $tjH$  is almost eliminated by the diphoton invariant mass cut, and  $t\bar{t}H$  is significantly reduced by the same cut. After the energy cut, both  $t\bar{t}\gamma$  and  $b\bar{b}\gamma\gamma$  are nearly eliminated. Finally, the remaining backgrounds include  $t\bar{t}\gamma\gamma$ ,  $tj\gamma\gamma$ ,  $Wjj\gamma\gamma$ , and a small amount of  $t\bar{t}H$ .

In the analysis of the Monte Carlo simulation results, the statistical significance is evaluated using the Poisson formula [118]:

$$\mathcal{S} = \sqrt{2L[(S+B)\ln(1+S/B) - S]}, \quad (5.24)$$

where  $S$  and  $B$  are cross sections of signal and background, respectively, while  $L$  represents the integrated luminosity. With an integrated luminosity of  $L = 300 \text{ fb}^{-1}$ , the statistical significance of the benchmark point P1 from Table 1 can reach  $1.1\sigma$  at the HL-LHC,  $1.5\sigma$  at the HE-LHC, and  $5.0\sigma$  at the FCC-hh, respectively. It is evident that, for the same integrated luminosity, a higher collider energy leads to a greater statistical significance.

In Fig. 6, the statistical significance of the surviving samples is shown in the  $\tan\beta$  versus  $\alpha$  plane for the 14 TeV HL-LHC with an integrated luminosity of  $L = 3 \text{ ab}^{-1}$  (left), the 27 TeV HE-LHC with  $L = 10 \text{ ab}^{-1}$  (middle), and the 100 TeV FCC-hh with  $L = 30 \text{ ab}^{-1}$  (right). According to the Monte Carlo simulation results, achieving a  $5\sigma$  discovery significance at the HL-LHC with  $L = 3 \text{ ab}^{-1}$  requires the cross section of the process  $pp \rightarrow t\bar{t}(h \rightarrow \gamma\gamma)$  to be at least 0.3 fb. However, in our parameter scan, the maximum cross section obtained for the surviving samples at the HL-LHC is approximately 0.23 fb. As a result, reaching  $5\sigma$  significance for this channel at the HL-LHC is challenging. In contrast, the prospects are much better at the HE-LHC and FCC-hh. To achieve  $5\sigma$  significance with the same integrated luminosity, the required cross sections are 0.67 fb and 2.36 fb, respectively, both of which are easily satisfied by the surviving samples. On the other hand, to reach  $2\sigma$  and  $5\sigma$  statistical significance at the 14 TeV HL-LHC, the required integrated luminosity are  $L = 764 \text{ fb}^{-1}$  and  $L = 4.8 \text{ ab}^{-1}$ , respectively. Comparable sensitivities can be achieved at the 27 TeV HE-LHC with  $L = 390 \text{ fb}^{-1}$  and  $L = 2.4 \text{ ab}^{-1}$ , and at the 100 TeV FCC-hh with only  $L = 36 \text{ fb}^{-1}$  and  $L = 227 \text{ fb}^{-1}$ , respectively.

With increasing collision energy and integrated luminosity, most of the surviving samples can be probed at the  $2\sigma$  or even  $5\sigma$  level at the 100 TeV FCC-hh with an integrated luminosity of  $L = 30 \text{ ab}^{-1}$ . However, there remain some surviving samples with the alignment condition  $\alpha \approx 1.25$  (corresponding to  $\sin(\beta - \alpha) \approx 0$ ) that are difficult to probe even at the  $2\sigma$  level, even further increases in energy and luminosity. This is because these samples exhibit highly suppressed diphoton decay rates, making them challenging to detect in this channel. As a result, alternative search channels or complementary methods are required to test these scenarios.

## 6 Conclusions

In this study, we investigated the potential of the Type-I 2HDM to account for the 95 GeV diphoton excess observed at the LHC, under current theoretical and experimental constraints. The impacts of various experimental data on the model parameters were analyzed in detail. Our parameter space scan shows that the 2HDM-I can successfully accommodate the observed excess. Monte Carlo simulations were then performed to assess the discovery potential of a 95 GeV Higgs boson at future hadron colliders. Particular attention was given to the process  $pp \rightarrow t(\rightarrow W^+b)\bar{t}(\rightarrow W^-\bar{b})h(\rightarrow \gamma\gamma)$ , where the Higgs

boson is produced in association with a top-quark pair and decays into diphotons. The simulation results indicate that a large portion of the viable parameter space can be effectively probed at future colliders via the top-associated diphoton channel.

Based on our analysis, the following conclusions are drawn about the 95 GeV Higgs boson in the 2HDM-I:

- The analysis reveals that direct Higgs search data impose strong constraints on the model parameter  $\alpha$ , excluding samples with  $\alpha \lesssim 0.95$ . Constraints from B-physics, particularly the branching ratio of  $B \rightarrow X_s \gamma$ , require  $\tan \beta \gtrsim 2.6$ . In addition, samples satisfying  $|m_{12}| \gtrsim 18 m_A - 400$  GeV and  $|m_{12}| \lesssim 18 m_A + 600$  GeV can yield a  $\Delta a_\mu$  consistent with the observed muon anomalous magnetic moment, potentially accounting for the discrepancy between theory and observation.
- The branching ratio of the lighter Higgs boson decaying into diphotons,  $\text{Br}(h \rightarrow \gamma\gamma)$ , primarily depends on the parameters  $\alpha$  and  $\tan \beta$ . It reaches a maximum of approximately  $10^{-2}$  with  $\sin(\beta - \alpha) \approx -0.2$ , and a minimum of about  $10^{-6}$  around the alignment limit  $\sin(\beta - \alpha) \approx 0$ . Meanwhile, both the production cross section  $\sigma(gg \rightarrow h)$  and the reduced top-Higgs coupling  $(C_{tth}/C_{tth}^{\text{SM}})^2$  exhibit similar dependence on  $\alpha$  and  $\tan \beta$ , being approximately proportional to  $\cos^2 \alpha$  and inversely proportional to  $\sin^2 \beta$ . The 95 GeV diphoton excess observed by CMS and ATLAS can be explained within  $1\sigma$  for samples around  $\sin(\beta - \alpha) \approx -0.2$  or  $\sin(\beta - \alpha) \approx 0.35$ .
- For the surviving samples, the maximum cross sections of the process  $pp \rightarrow t\bar{t}(h \rightarrow \gamma\gamma)$  at the HL-LHC, HE-LHC, and FCC-hh can reach 0.23 fb, 0.75 fb, and 9.07 fb, respectively. The dominant SM backgrounds for this channel arise from the processes  $t\bar{t}\gamma$ ,  $b\bar{b}\gamma\gamma$ , and  $Wjj\gamma\gamma$ .
- The Monte Carlo simulation results indicate that, for a fixed integrated luminosity, a higher collider energy leads to a greater statistical significance. For the HL-LHC with  $L = 3 \text{ ab}^{-1}$ , achieving over  $5\sigma$  significance in  $pp \rightarrow t\bar{t}(h \rightarrow \gamma\gamma)$  channel requires a cross section exceeding 0.3 fb, which beyond the maximum that can be achieved. Nevertheless, to achieve  $5\sigma$  significance with the same integrated luminosities at HE-LHC and FCC-hh, the required cross sections are 0.67 fb and 2.36 fb, respectively, both of these values are easily satisfied by the surviving samples.
- A statistical significance of  $2\sigma$  can be reached at the HL-LHC with an integrated luminosity of  $L = 764 \text{ fb}^{-1}$ , whereas  $5\sigma$  cannot be achieved even at the design luminosity. In contrast, at the HE-LHC,  $2\sigma$  and  $5\sigma$  significance levels can be reached with  $L = 390 \text{ fb}^{-1}$  and  $L = 2.4 \text{ ab}^{-1}$ , respectively. The same levels of significance can be obtained at the FCC-hh with much lower luminosities:  $L = 36 \text{ fb}^{-1}$  for  $2\sigma$ , and  $L = 227 \text{ fb}^{-1}$  for  $5\sigma$ .
- Samples located in the region  $\sin(\beta - \alpha) \approx 0$  are difficult to probe even at the  $2\sigma$  level, despite further increases in collision energy and integrated luminosity. This is due to the suppression of the coupling  $C_{hWW}$  in this region, which significantly reduces the

diphoton decay rate of the light Higgs boson. Such scenarios may therefore need to be tested through alternative production or decay channels.

## Acknowledgments

This work was supported by the National Natural Science Foundation of China under Grant No. 12275066 and by the startup research funds of Henan University.

**Note added.** During the preparation of this manuscript, a paper with a comparable analysis was published on arXiv [10]. What's apart is that it starts from theory to explain experimental anomalies, whereas we place a greater emphasis on testing the model at future colliders.

## References

- [1] CMS collaboration, *Observation of a New Boson at a Mass of 125 GeV with the CMS Experiment at the LHC*, *Phys. Lett. B* **716** (2012) 30 [[1207.7235](#)].
- [2] ATLAS collaboration, *Observation of a new particle in the search for the Standard Model Higgs boson with the ATLAS detector at the LHC*, *Phys. Lett. B* **716** (2012) 1 [[1207.7214](#)].
- [3] CMS collaboration, *A portrait of the Higgs boson by the CMS experiment ten years after the discovery.*, *Nature* **607** (2022) 60 [[2207.00043](#)].
- [4] ATLAS collaboration, *A detailed map of Higgs boson interactions by the ATLAS experiment ten years after the discovery*, *Nature* **607** (2022) 52 [[2207.00092](#)].
- [5] LEP WORKING GROUP FOR HIGGS BOSON SEARCHES, ALEPH, DELPHI, L3, OPAL collaboration, *Search for the standard model Higgs boson at LEP*, *Phys. Lett. B* **565** (2003) 61 [[hep-ex/0306033](#)].
- [6] CMS collaboration, *Search for a standard model-like Higgs boson in the mass range between 70 and 110 GeV in the diphoton final state in proton-proton collisions at  $\sqrt{s} = 8$  and 13 TeV*, *Phys. Lett. B* **793** (2019) 320 [[1811.08459](#)].
- [7] ATLAS collaboration, *Search for diphoton resonances in the 66 to 110 GeV mass range using pp collisions at  $\sqrt{s} = 13$  TeV with the ATLAS detector*, *CERN-EP-2024-166* (2024) [[2407.07546](#)].
- [8] CMS collaboration, *Search for a standard model-like Higgs boson in the mass range between 70 and 110 GeV in the diphoton final state in proton-proton collisions at  $\sqrt{s} = 13$  TeV*, *CMS-HIG-20-002*, *CERN-EP-2024-088* (2024) [[2405.18149](#)].
- [9] D. Azevedo, T. Biekötter and P.M. Ferreira, *2HDM interpretations of the CMS diphoton excess at 95 GeV*, *JHEP* **11** (2023) 017 [[2305.19716](#)].
- [10] A. Khanna, S. Moretti and A. Sarkar, *Explaining 95 (or so) GeV Anomalies in the 2-Higgs Doublet Model Type-I*, [2409.02587](#).
- [11] R. Benbrik, M. Boukidi and S. Moretti, *Superposition of CP-Even and CP-Odd Higgs Resonances: Explaining the 95 GeV Excesses within a Two-Higgs Doublet Model*, [2405.02899](#).

- [12] A. Belyaev, R. Benbrik, M. Boukidi, M. Chakraborti, S. Moretti and S. Semlali, *Explanation of the hints for a 95 GeV Higgs boson within a 2-Higgs Doublet Model*, *JHEP* **05** (2024) 209 [[2306.09029](#)].
- [13] R. Benbrik, M. Boukidi, S. Moretti and S. Semlali, *Explaining the 96 GeV Di-photon anomaly in a generic 2HDM Type-III*, *Phys. Lett. B* **832** (2022) 137245 [[2204.07470](#)].
- [14] S. Ashanujjaman, S. Banik, G. Coloretti, A. Crivellin, B. Mellado and A.-T. Mulaudzi, *SU(2)<sub>L</sub> triplet scalar as the origin of the 95 GeV excess?*, *Phys. Rev. D* **108** (2023) L091704 [[2306.15722](#)].
- [15] Z.-f. Ge, F.-Y. Niu and J.-L. Yang, *The origin of the 95 GeV excess in the flavor-dependent U(1)<sub>X</sub> model*, *Eur. Phys. J. C* **84** (2024) 548 [[2405.07243](#)].
- [16] A. Ahriche, M.L. Bellilet, M.O. Khojali, M. Kumar and A.-T. Mulaudzi, *Scale invariant scotogenic model: CDF-II W-boson mass and the 95 GeV excesses*, *Phys. Rev. D* **110** (2024) 015025 [[2311.08297](#)].
- [17] P.S.B. Dev, R.N. Mohapatra and Y. Zhang, *Explanation of the 95 GeV  $\gamma\gamma$  and  $bb^{-}$  excesses in the minimal left-right symmetric model*, *Phys. Lett. B* **849** (2024) 138481 [[2312.17733](#)].
- [18] A. Kundu, S. Maharana and P. Mondal, *A 96 GeV scalar tagged to dark matter models*, *Nucl. Phys. B* **955** (2020) 115057 [[1907.12808](#)].
- [19] J.A. Aguilar-Saavedra and F.R. Joaquim, *Multiphoton signals of a (96 GeV?) stealth boson*, *Eur. Phys. J. C* **80** (2020) 403 [[2002.07697](#)].
- [20] S. Yaser Ayazi, M. Hosseini, S. Paktinat Mehdiabadi and R. Rouzbehi, *Vector dark matter and LHC constraints, including a 95 GeV light Higgs boson*, *Phys. Rev. D* **110** (2024) 055004 [[2405.01132](#)].
- [21] L. Liu, H. Qiao, K. Wang and J. Zhu, *A Light Scalar in the Minimal Dilaton Model in Light of LHC Constraints*, *Chin. Phys. C* **43** (2019) 023104 [[1812.00107](#)].
- [22] K. Wang and J. Zhu, *95 GeV light Higgs in the top-pair-associated diphoton channel at the LHC in the minimal dilaton model\**, *Chin. Phys. C* **48** (2024) 073105 [[2402.11232](#)].
- [23] S. Heinemeyer, C. Li, F. Lika, G. Moortgat-Pick and S. Paasch, *Phenomenology of a 96 GeV Higgs boson in the 2HDM with an additional singlet*, *Phys. Rev. D* **106** (2022) 075003 [[2112.11958](#)].
- [24] T. Biekötter and M.O. Olea-Romacho, *Reconciling Higgs physics and pseudo-Nambu-Goldstone dark matter in the S2HDM using a genetic algorithm*, *JHEP* **10** (2021) 215 [[2108.10864](#)].
- [25] T. Biekötter, S. Heinemeyer and G. Weiglein, *The CMS di-photon excess at 95 GeV in view of the LHC Run 2 results*, *Phys. Lett. B* **846** (2023) 138217 [[2303.12018](#)].
- [26] T. Biekötter, S. Heinemeyer and G. Weiglein, *95.4 GeV diphoton excess at ATLAS and CMS*, *Phys. Rev. D* **109** (2024) 035005 [[2306.03889](#)].
- [27] G. Arcadi, G. Busoni, D. Cabo-Almeida and N. Krishnan, *Is there a (Pseudo)Scalar at 95 GeV?*, [2311.14486](#).
- [28] T. Biekötter, M. Chakraborti and S. Heinemeyer, *A 96 GeV Higgs boson in the N2HDM*, *Eur. Phys. J. C* **80** (2020) 2 [[1903.11661](#)].
- [29] T. Biekötter, A. Grohsjean, S. Heinemeyer, C. Schwanenberger and G. Weiglein, *Possible*

indications for new Higgs bosons in the reach of the LHC:  $N2HDM$  and  $NMSSM$  interpretations, *Eur. Phys. J. C* **82** (2022) 178 [2109.01128].

- [30] S. Banik, A. Crivellin, S. Iguro and T. Kitahara, *Asymmetric di-Higgs signals of the next-to-minimal 2HDM with a  $U(1)$  symmetry*, *Phys. Rev. D* **108** (2023) 075011 [2303.11351].
- [31] J.A. Aguilar-Saavedra, H.B. Câmara, F.R. Joaquim and J.F. Seabra, *Confronting the 95 GeV excesses within the  $U(1)$ '-extended next-to-minimal 2HDM*, *Phys. Rev. D* **108** (2023) 075020 [2307.03768].
- [32] C. Wang, J.-Q. Tao, M.A. Shahzad, G.-M. Chen and S. Gascon-Shotkin, *Search for a lighter neutral custodial fiveplet scalar in the Georgi-Machacek model \**, *Chin. Phys. C* **46** (2022) 083107 [2204.09198].
- [33] T.-K. Chen, C.-W. Chiang, S. Heinemeyer and G. Weiglein, *95 GeV Higgs boson in the Georgi-Machacek model*, *Phys. Rev. D* **109** (2024) 075043 [2312.13239].
- [34] A. Ahriche, *95 GeV excess in the Georgi-Machacek model: Single or twin peak resonance*, *Phys. Rev. D* **110** (2024) 035010 [2312.10484].
- [35] J. Cao, X. Guo, Y. He, P. Wu and Y. Zhang, *Diphoton signal of the light Higgs boson in natural NMSSM*, *Phys. Rev. D* **95** (2017) 116001 [1612.08522].
- [36] J. Cao, X. Jia, Y. Yue, H. Zhou and P. Zhu, *96 GeV diphoton excess in seesaw extensions of the natural NMSSM*, *Phys. Rev. D* **101** (2020) 055008 [1908.07206].
- [37] W.G. Hollik, C. Li, G. Moortgat-Pick and S. Paasch, *Phenomenology of a Supersymmetric Model Inspired by Inflation*, *Eur. Phys. J. C* **81** (2021) 141 [2004.14852].
- [38] W. Li, H. Qiao and J. Zhu, *Light Higgs boson in the NMSSM confronted with the CMS di-photon and di-tau excesses\**, *Chin. Phys. C* **47** (2023) 123102 [2212.11739].
- [39] F. Domingo, U. Ellwanger and C. Hugonie,  *$M_W$ , dark matter and  $a_\mu$  in the NMSSM*, *Eur. Phys. J. C* **82** (2022) 1074 [2209.03863].
- [40] J. Cao, X. Jia, J. Lian and L. Meng, *95 GeV diphoton and  $bb^-$  excesses in the general next-to-minimal supersymmetric standard model*, *Phys. Rev. D* **109** (2024) 075001 [2310.08436].
- [41] W. Li, H. Qiao, K. Wang and J. Zhu, *Light dark matter confronted with the 95 GeV diphoton excess*, 2312.17599.
- [42] J. Lian, *The 95 GeV Excesses in the  $\mathbb{Z}_3$ -symmetric Next-to Minimal Supersymmetric Standard Model*, 2406.10969.
- [43] J. Cao, X. Jia and J. Lian, *Unified Interpretation of Muon  $g-2$  anomaly, 95 GeV Diphoton, and  $b\bar{b}$  Excesses in the General Next-to-Minimal Supersymmetric Standard Model*, 2402.15847.
- [44] U. Ellwanger and C. Hugonie, *Additional Higgs Bosons near 95 and 650 GeV in the NMSSM*, *Eur. Phys. J. C* **83** (2023) 1138 [2309.07838].
- [45] U. Ellwanger, C. Hugonie, S.F. King and S. Moretti, *NMSSM explanation for excesses in the search for neutralinos and charginos and a 95 GeV Higgs boson*, *Eur. Phys. J. C* **84** (2024) 788 [2404.19338].
- [46] K. Wang, F. Wang, J. Zhu and Q. Jie, *The semi-constrained NMSSM in light of muon  $g-2$ , LHC, and dark matter constraints*, *Chin. Phys. C* **42** (2018) 103109 [1811.04435].

- [47] T.D. Lee, *A Theory of Spontaneous T Violation*, *Phys. Rev. D* **8** (1973) 1226.
- [48] G.C. Branco, P.M. Ferreira, L. Lavoura, M.N. Rebelo, M. Sher and J.P. Silva, *Theory and phenomenology of two-Higgs-doublet models*, *Phys. Rept.* **516** (2012) 1 [[1106.0034](#)].
- [49] D. Atwood, L. Reina and A. Soni, *Phenomenology of two Higgs doublet models with flavor changing neutral currents*, *Phys. Rev. D* **55** (1997) 3156 [[hep-ph/9609279](#)].
- [50] J.F. Gunion and H.E. Haber, *The CP conserving two Higgs doublet model: The Approach to the decoupling limit*, *Phys. Rev. D* **67** (2003) 075019 [[hep-ph/0207010](#)].
- [51] G. Bhattacharyya and D. Das, *Scalar sector of two-Higgs-doublet models: A minireview*, *Pramana* **87** (2016) 40 [[1507.06424](#)].
- [52] L. Wang, J.M. Yang and Y. Zhang, *Two-Higgs-doublet models in light of current experiments: a brief review*, *Commun. Theor. Phys.* **74** (2022) 097202 [[2203.07244](#)].
- [53] H.E. Haber and G.L. Kane, *The Search for Supersymmetry: Probing Physics Beyond the Standard Model*, *Phys. Rept.* **117** (1985) 75.
- [54] A. Pich and P. Tuzon, *Yukawa Alignment in the Two-Higgs-Doublet Model*, *Phys. Rev. D* **80** (2009) 091702 [[0908.1554](#)].
- [55] P. Tuzon and A. Pich, *The Aligned two-Higgs Doublet model*, *Acta Phys. Polon. Supp.* **3** (2010) 215 [[1001.0293](#)].
- [56] H.E. Haber, G.L. Kane and T. Sterling, *The Fermion Mass Scale and Possible Effects of Higgs Bosons on Experimental Observables*, *Nucl. Phys. B* **161** (1979) 493.
- [57] L.J. Hall and M.B. Wise, *FLAVOR CHANGING HIGGS - BOSON COUPLINGS*, *Nucl. Phys. B* **187** (1981) 397.
- [58] A. Arhrib, R. Benbrik, R. Enberg, W. Klemm, S. Moretti and S. Munir, *Identifying a light charged Higgs boson at the LHC Run II*, *Phys. Lett. B* **774** (2017) 591 [[1706.01964](#)].
- [59] Y. Wang, A. Arhrib, R. Benbrik, M. Krab, B. Manaut, S. Moretti et al., *Analysis of  $W + 4\gamma$  in the 2HDM Type-I at the LHC*, *JHEP* **12** (2021) 021 [[2107.01451](#)].
- [60] P. Posch, *Enhancement of  $h \rightarrow \gamma\gamma$  in the Two Higgs Doublet Model Type I*, *Phys. Lett. B* **696** (2011) 447 [[1001.1759](#)].
- [61] ATLAS collaboration, *Measurement of Higgs boson decay into b-quarks in associated production with a top-quark pair in pp collisions at  $\sqrt{s} = 13$  TeV with the ATLAS detector*, *JHEP* **06** (2022) 097 [[2111.06712](#)].
- [62] ATLAS collaboration, *Measurement of the associated production of a top-antitop-quark pair and a Higgs boson decaying into a  $b\bar{b}$  pair in pp collisions at  $\sqrt{s} = 13$  TeV using the ATLAS detector at the LHC*, [2407.10904](#).
- [63] M. Aoki, S. Kanemura, K. Tsumura and K. Yagyu, *Models of Yukawa interaction in the two Higgs doublet model, and their collider phenomenology*, *Phys. Rev. D* **80** (2009) 015017 [[0902.4665](#)].
- [64] M. Carena and H.E. Haber, *Higgs Boson Theory and Phenomenology*, *Prog. Part. Nucl. Phys.* **50** (2003) 63 [[hep-ph/0208209](#)].
- [65] A. Djouadi, *The Anatomy of electro-weak symmetry breaking. II. The Higgs bosons in the minimal supersymmetric model*, *Phys. Rept.* **459** (2008) 1 [[hep-ph/0503173](#)].

- [66] Y. Bai, V. Barger, L.L. Everett and G. Shaughnessy, *General two Higgs doublet model (2HDM-G) and Large Hadron Collider data*, *Phys. Rev. D* **87** (2013) 115013 [[1210.4922](#)].
- [67] F. Staub, *From Superpotential to Model Files for FeynArts and CalcHep/CompHep*, *Comput. Phys. Commun.* **181** (2010) 1077 [[0909.2863](#)].
- [68] F. Staub, *Automatic Calculation of supersymmetric Renormalization Group Equations and Self Energies*, *Comput. Phys. Commun.* **182** (2011) 808 [[1002.0840](#)].
- [69] F. Staub, *SARAH 3.2: Dirac Gauginos, UFO output, and more*, *Comput. Phys. Commun.* **184** (2013) 1792 [[1207.0906](#)].
- [70] F. Staub, *SARAH 4 : A tool for (not only SUSY) model builders*, *Comput. Phys. Commun.* **185** (2014) 1773 [[1309.7223](#)].
- [71] W. Porod, *SPheno, a program for calculating supersymmetric spectra, SUSY particle decays and SUSY particle production at  $e^+ e^-$  colliders*, *Comput. Phys. Commun.* **153** (2003) 275 [[hep-ph/0301101](#)].
- [72] W. Porod and F. Staub, *SPheno 3.1: Extensions including flavour, CP-phases and models beyond the MSSM*, *Comput. Phys. Commun.* **183** (2012) 2458 [[1104.1573](#)].
- [73] ATLAS collaboration, *Study of the rare decays of  $B_s^0$  and  $B^0$  mesons into muon pairs using data collected during 2015 and 2016 with the ATLAS detector*, *JHEP* **04** (2019) 098 [[1812.03017](#)].
- [74] CMS collaboration, *Measurement of properties of  $B_s^0 \rightarrow \mu^+ \mu^-$  decays and search for  $B^0 \rightarrow \mu^+ \mu^-$  with the CMS experiment*, *JHEP* **04** (2020) 188 [[1910.12127](#)].
- [75] LHCb collaboration, *Analysis of Neutral B-Meson Decays into Two Muons*, *Phys. Rev. Lett.* **128** (2022) 041801 [[2108.09284](#)].
- [76] HFLAV collaboration, *Averages of b-hadron, c-hadron, and  $\tau$ -lepton properties as of 2021*, *Phys. Rev. D* **107** (2023) 052008 [[2206.07501](#)].
- [77] PARTICLE DATA GROUP collaboration, *Review of Particle Physics*, *PTEP* **2022** (2022) 083C01.
- [78] F. Mahmoudi, *SuperIso: A Program for calculating the isospin asymmetry of  $B \rightarrow K^* \gamma$  in the MSSM*, *Comput. Phys. Commun.* **178** (2008) 745 [[0710.2067](#)].
- [79] F. Mahmoudi, *SuperIso v2.3: A Program for calculating flavor physics observables in Supersymmetry*, *Comput. Phys. Commun.* **180** (2009) 1579 [[0808.3144](#)].
- [80] T. Aoyama et al., *The anomalous magnetic moment of the muon in the Standard Model*, *Phys. Rept.* **887** (2020) 1 [[2006.04822](#)].
- [81] MUON G-2 collaboration, *Measurement of the Positive Muon Anomalous Magnetic Moment to 0.20 ppm*, *Phys. Rev. Lett.* **131** (2023) 161802 [[2308.06230](#)].
- [82] PARTICLE DATA GROUP collaboration, *Review of particle physics*, *Phys. Rev. D* **110** (2024) 030001.
- [83] P. Athron, M. Bach, H.G. Fargnoli, C. Gnendiger, R. Greifenhagen, J.-h. Park et al., *GM2Calc: Precise MSSM prediction for  $(g - 2)$  of the muon*, *Eur. Phys. J. C* **76** (2016) 62 [[1510.08071](#)].
- [84] P. Athron, C. Balazs, A. Cherchiglia, D.H.J. Jacob, D. Stöckinger, H. Stöckinger-Kim et al., *Two-loop prediction of the anomalous magnetic moment of the muon in the Two-Higgs Doublet Model with GM2Calc 2*, *Eur. Phys. J. C* **82** (2022) 229 [[2110.13238](#)].

- [85] LEP collaboration, *Searches for Higgs Bosons Decaying into Photons : Combined Results from the LEP Experiments, DELPHI-2002-087 CONF 620, CERN-ALEPH-2002-019, CERN-ALEPH-CONF-2002-008* (2002) .
- [86] ATLAS collaboration, *Search for Scalar Diphoton Resonances in the Mass Range 65 – 600 GeV with the ATLAS Detector in pp Collision Data at  $\sqrt{s} = 8$  TeV*, *Phys. Rev. Lett.* **113** (2014) 171801 [[1407.6583](#)].
- [87] CMS collaboration, *Search for new resonances in the diphoton final state in the mass range between 80 and 115 GeV in pp collisions at  $\sqrt{s} = 8$  TeV*, *CMS-PAS-HIG-14-037* (2015) .
- [88] P. Bechtle, D. Dercks, S. Heinemeyer, T. Klingl, T. Stefaniak, G. Weiglein et al., *HiggsBounds-5: Testing Higgs Sectors in the LHC 13 TeV Era*, *Eur. Phys. J. C* **80** (2020) 1211 [[2006.06007](#)].
- [89] P. Bechtle, S. Heinemeyer, T. Klingl, T. Stefaniak, G. Weiglein and J. Wittbrodt, *HiggsSignals-2: Probing new physics with precision Higgs measurements in the LHC 13 TeV era*, *Eur. Phys. J. C* **81** (2021) 145 [[2012.09197](#)].
- [90] M.E. Peskin and T. Takeuchi, *A New constraint on a strongly interacting Higgs sector*, *Phys. Rev. Lett.* **65** (1990) 964.
- [91] M.E. Peskin and T. Takeuchi, *Estimation of oblique electroweak corrections*, *Phys. Rev. D* **46** (1992) 381.
- [92] S. Kanemura, T. Kubota and E. Takasugi, *Lee-Quigg-Thacker bounds for Higgs boson masses in a two doublet model*, *Phys. Lett. B* **313** (1993) 155 [[hep-ph/9303263](#)].
- [93] A.G. Akeroyd, A. Arhrib and E.-M. Naimi, *Note on tree level unitarity in the general two Higgs doublet model*, *Phys. Lett. B* **490** (2000) 119 [[hep-ph/0006035](#)].
- [94] A. Arhrib, *Unitarity constraints on scalar parameters of the standard and two Higgs doublets model*, in *Workshop on Noncommutative Geometry, Superstrings and Particle Physics*, 12, 2000 [[hep-ph/0012353](#)].
- [95] A.W. El Kaffas, W. Khater, O.M. Ogreid and P. Osland, *Consistency of the two Higgs doublet model and CP violation in top production at the LHC*, *Nucl. Phys. B* **775** (2007) 45 [[hep-ph/0605142](#)].
- [96] Y.-F. Zhou and Y.-L. Wu, *Lepton flavor changing scalar interactions and muon  $g-2$* , *Eur. Phys. J. C* **27** (2003) 577 [[hep-ph/0110302](#)].
- [97] K.A. Assamagan, A. Deandrea and P.-A. Delsart, *Search for the lepton flavor violating decay  $A0 / H0 \rightarrow \tau\mu$  at hadron colliders*, *Phys. Rev. D* **67** (2003) 035001 [[hep-ph/0207302](#)].
- [98] S. Davidson and G.J. Grenier, *Lepton flavour violating Higgs and tau to mu gamma*, *Phys. Rev. D* **81** (2010) 095016 [[1001.0434](#)].
- [99] X.-F. Han, F. Wang, L. Wang, J.M. Yang and Y. Zhang, *Joint explanation of W-mass and muon  $g-2$  in the 2HDM\**, *Chin. Phys. C* **46** (2022) 103105 [[2204.06505](#)].
- [100] A. Cherchiglia, P. Kneschke, D. Stöckinger and H. Stöckinger-Kim, *The muon magnetic moment in the 2HDM: complete two-loop result*, *JHEP* **01** (2017) 007 [[1607.06292](#)].
- [101] A. Cherchiglia, D. Stöckinger and H. Stöckinger-Kim, *Muon  $g-2$  in the 2HDM: maximum results and detailed phenomenology*, *Phys. Rev. D* **98** (2018) 035001 [[1711.11567](#)].

- [102] S.-P. Li, X.-Q. Li, Y.-Y. Li, Y.-D. Yang and X. Zhang, *Power-aligned 2HDM: a correlative perspective on  $(g - 2)_{e,\mu}$* , *JHEP* **01** (2021) 034 [[2010.02799](#)].
- [103] LHC HIGGS CROSS SECTION WORKING GROUP collaboration, *Handbook of LHC Higgs Cross Sections: 1. Inclusive Observables*, *CERN-2011-002* (2011) [[1101.0593](#)].
- [104] LHC HIGGS CROSS SECTION WORKING GROUP collaboration, *Handbook of LHC Higgs Cross Sections: 3. Higgs Properties*, [1307.1347](#).
- [105] J. Alwall, M. Herquet, F. Maltoni, O. Mattelaer and T. Stelzer, *MadGraph 5 : Going Beyond*, *JHEP* **06** (2011) 128 [[1106.0522](#)].
- [106] J. Alwall, R. Frederix, S. Frixione, V. Hirschi, F. Maltoni, O. Mattelaer et al., *The automated computation of tree-level and next-to-leading order differential cross sections, and their matching to parton shower simulations*, *JHEP* **07** (2014) 079 [[1405.0301](#)].
- [107] CMS collaboration, *Performance of Photon Reconstruction and Identification with the CMS Detector in Proton-Proton Collisions at  $\sqrt{s} = 8$  TeV*, *JINST* **10** (2015) P08010 [[1502.02702](#)].
- [108] Z. Abdy and M. Mohammadi Najafabadi, *Prospect study for the measurement of the  $Hbb^{-}$  coupling at the LHC and FCC-hh*, *Phys. Rev. D* **109** (2024) 093003 [[2405.02667](#)].
- [109] NNPDF collaboration, *Parton distributions for the LHC Run II*, *JHEP* **04** (2015) 040 [[1410.8849](#)].
- [110] A. Buckley, J. Ferrando, S. Lloyd, K. Nordström, B. Page, M. Rüfenacht et al., *LHAPDF6: parton density access in the LHC precision era*, *Eur. Phys. J. C* **75** (2015) 132 [[1412.7420](#)].
- [111] T. Sjöstrand, S. Ask, J.R. Christiansen, R. Corke, N. Desai, P. Ilten et al., *An introduction to PYTHIA 8.2*, *Comput. Phys. Commun.* **191** (2015) 159 [[1410.3012](#)].
- [112] M. Cacciari, G.P. Salam and G. Soyez, *The anti- $k_t$  jet clustering algorithm*, *JHEP* **04** (2008) 063 [[0802.1189](#)].
- [113] DELPHES 3 collaboration, *DELPHES 3, A modular framework for fast simulation of a generic collider experiment*, *JHEP* **02** (2014) 057 [[1307.6346](#)].
- [114] M. Selvaggi, *DELPHES 3: A modular framework for fast-simulation of generic collider experiments*, *J. Phys. Conf. Ser.* **523** (2014) 012033.
- [115] E. Conte, B. Fuks and G. Serret, *MadAnalysis 5, A User-Friendly Framework for Collider Phenomenology*, *Comput. Phys. Commun.* **184** (2013) 222 [[1206.1599](#)].
- [116] M. Cepeda et al., *Report from Working Group 2: Higgs Physics at the HL-LHC and HE-LHC*, *CERN Yellow Rep. Monogr.* **7** (2019) 221 [[1902.00134](#)].
- [117] FCC collaboration, *FCC-hh: The Hadron Collider: Future Circular Collider Conceptual Design Report Volume 3*, *Eur. Phys. J. ST* **228** (2019) 755.
- [118] G. Cowan, K. Cranmer, E. Gross and O. Vitells, *Asymptotic formulae for likelihood-based tests of new physics*, *Eur. Phys. J. C* **71** (2011) 1554 [[1007.1727](#)].